Supporting Information
For

Atomistic Insights into Organization of RNA Loaded Lipid Nanoparticles

Markéta Paloncýová[*a], *Martin Šrejber*[a], *Petra Čechová*[a], *Petra Kührová*[a], *Filip Zaoral*[b], *and Michal Otyepka**[ab]

[a] Regional Center of Advanced Technologies and Materials, The Czech Advanced Technology and Research Institute (CATRIN), Palacký University Olomouc, Šlechtitelů 27, 779 00 Olomouc, Czech Republic

[b] IT4Innovations, VŠB – Technical University of Ostrava, 17. listopadu 2172/15, 708 00 Ostrava-Poruba, Czech Republic

Outline

Methods

CG parameterization

In order to perform simulations in coarse grained (CG) resolution, individual lipid species found in the LNPs were parametrized according to the MARTINI philosophy and in line with the newly derived MARTINI 3 force field[1] available at www.cgmartini.nl. In terms of the LNP composition, ILs and the PEGylated lipid species from Pfizer & BioNTech vaccome were studied, containing ALC-0315 (((4-hydroxybutyl)azanediyl)bis-(hexane-6,1-diyl)bis(2-hexyldecanoate)) and ALC-0159 (2-[(polyethylene glycol)-2000]-N,N-ditetradecylacetamide). Parameters of ILs were derived for both forms e.g. charged and neutral, reflecting conditions during LNPs preparation/loading and physiological state after administration. In addition to ILs and PEGylated lipids, cholesterol and di-saturated DPPC lipid (1,2-dipalmitoyl-*sn*-glycero-3-phosphocholine, model for DPPC and DSPC) were added to the system in line with COVID-19 vaccine composition.[2] Beta version of cholesterol parameters were provided to us by P. C. T. Souza.

Lipid parametrization

Prior to the CG parametrization of the abovementioned lipid species, each lipid was mapped into the CG resolution according to the general MARTINI philosophy, where approximately four heavy atoms (not including hydrogens) are considered as building blocks of so-called beads (Figure S1).

As the reference input for lipid CG parametrization, atomistic data from our previous publication[3] were used, containing simulations of pure lipid bilayers composed of ALC-0315 lipids in both charged/neutral forms as well as mixed membranes (with molar ratio of 50(IL – ALC-0315):38.5(Cholesterol):10(DSPC):1.5(PEGylated lipid – ALC-0159)). The last 50 ns of those atomistic simulations were used with total of 10000 frames per trajectory. Analysis was performed on ensembles of all lipids. Since all non-bonded parameters are unique for the individual bead types and are well described by the MARTINI interaction matrix, only the bonded parameters (namely bond lengths and angles) were subject to further parametrization. Dihedral angles were not parameterized, according to general practice for MARTINI lipid parameterization procedure. The procedure comprised of extraction of the bonded parameters from atomistic trajectories (analogous to the mapping scheme in *Figure S1*) and comparison with the newly designed CG parameters and their iterative refinements. To ensure the consistence between compared parameters, CG models of lipid bilayer corresponding to the composition of referenced atomistic membranes were created. Individual CG systems were simulated for total of 3 μs each time. Resulting comparison of bond and angle parameters are shown in *Figure S2-S7*. In case of the PEGylated lipids, only non-PEGylated parts of lipids were parametrized. The parameters for PEG chains were generated by the PolyPly software.[4] For simulations containing PEGylated lipids the interaction between SN3r and water (W) beads was modified (to ε=3.6 kJ/mol) as advised by authors. [https://github.com/marrink-lab/polyply_1.0/wiki/Tutorial:-PEGylated-lipid-bilayers] Topology files for all lipids can be found in online Zenodo repository (https://zenodo.org/record/7456781#.Y6w8wi8w1mB).

In the next section, the bead assignment and structural parameter comparisons of lipids between AA and CG systems are presented. The overlaps of the final bond and angle parameters are shown between all-atom and coarse grained simulations (Figs. S2-S7).

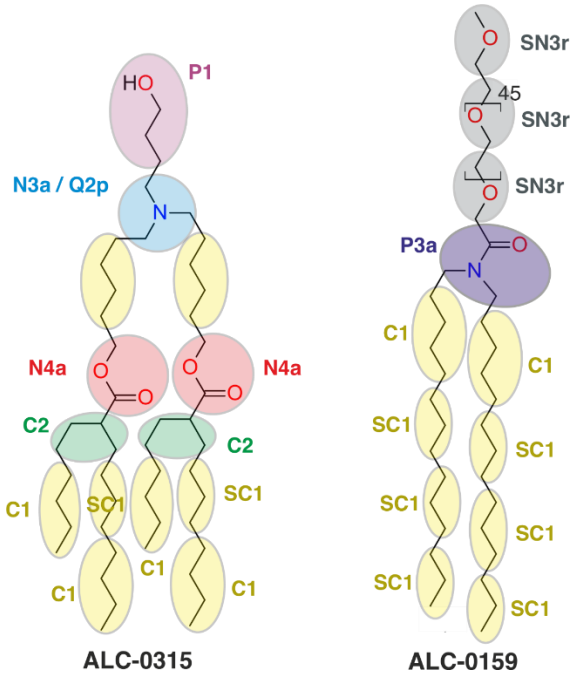

Figure S1. *Atomistic to coarse grained mapping scheme for ionizable (ALC-0315) and PEGylated (ALC-0159) lipids. In the case of ILs, bead types for both forms are shown (N3a – neutral, Q2p – charged).*

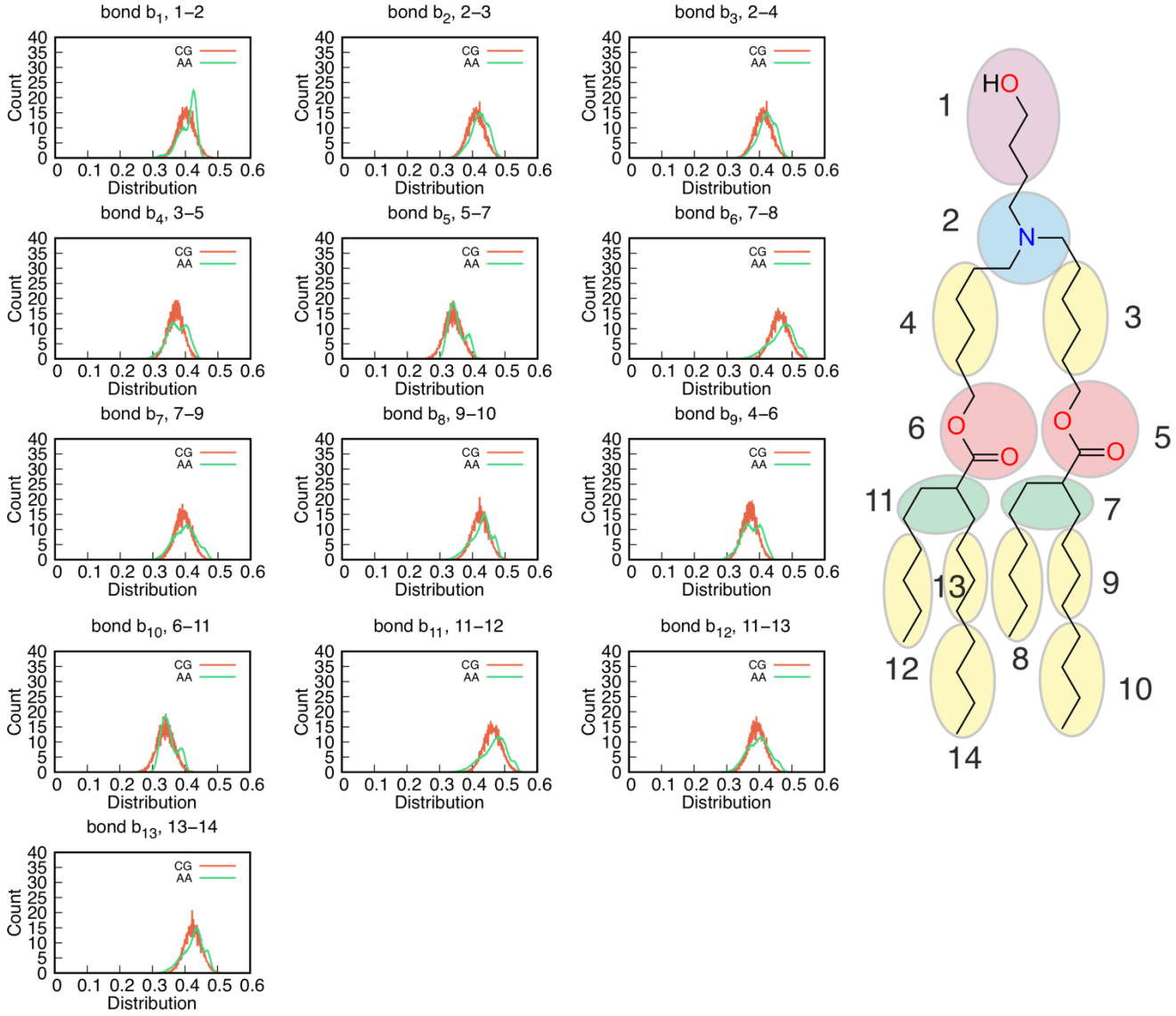

Figure S2. *The distributions of bond parameters extracted from all-atom (AA) and coarse grained (CG) simulations for ALC-0315 (charged) lipid.*

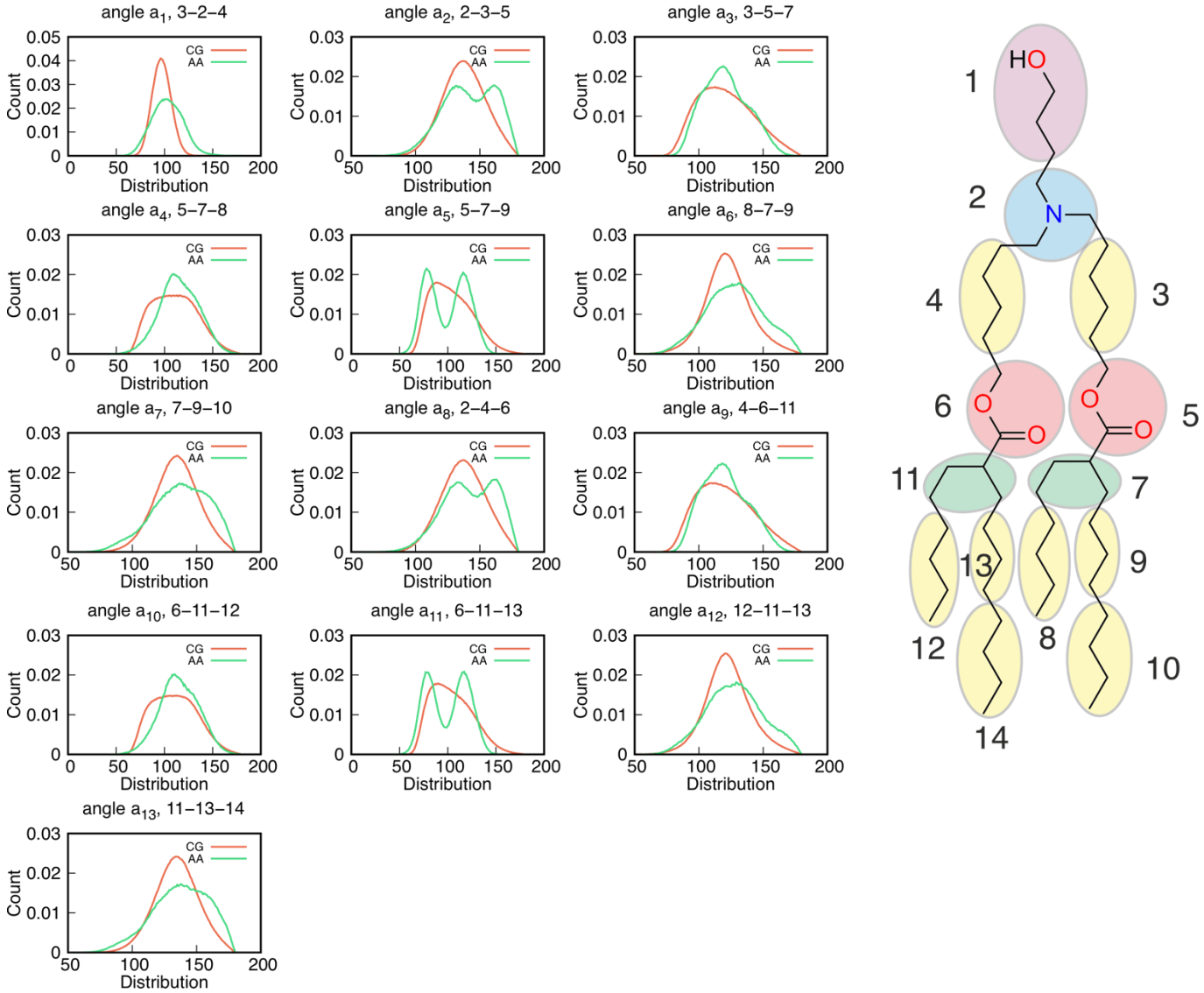

Figure S3. *The distributions of angle parameters extracted from all-atom (AA) and coarse grained (CG) simulations for ALC-0315 (charged) lipid.*

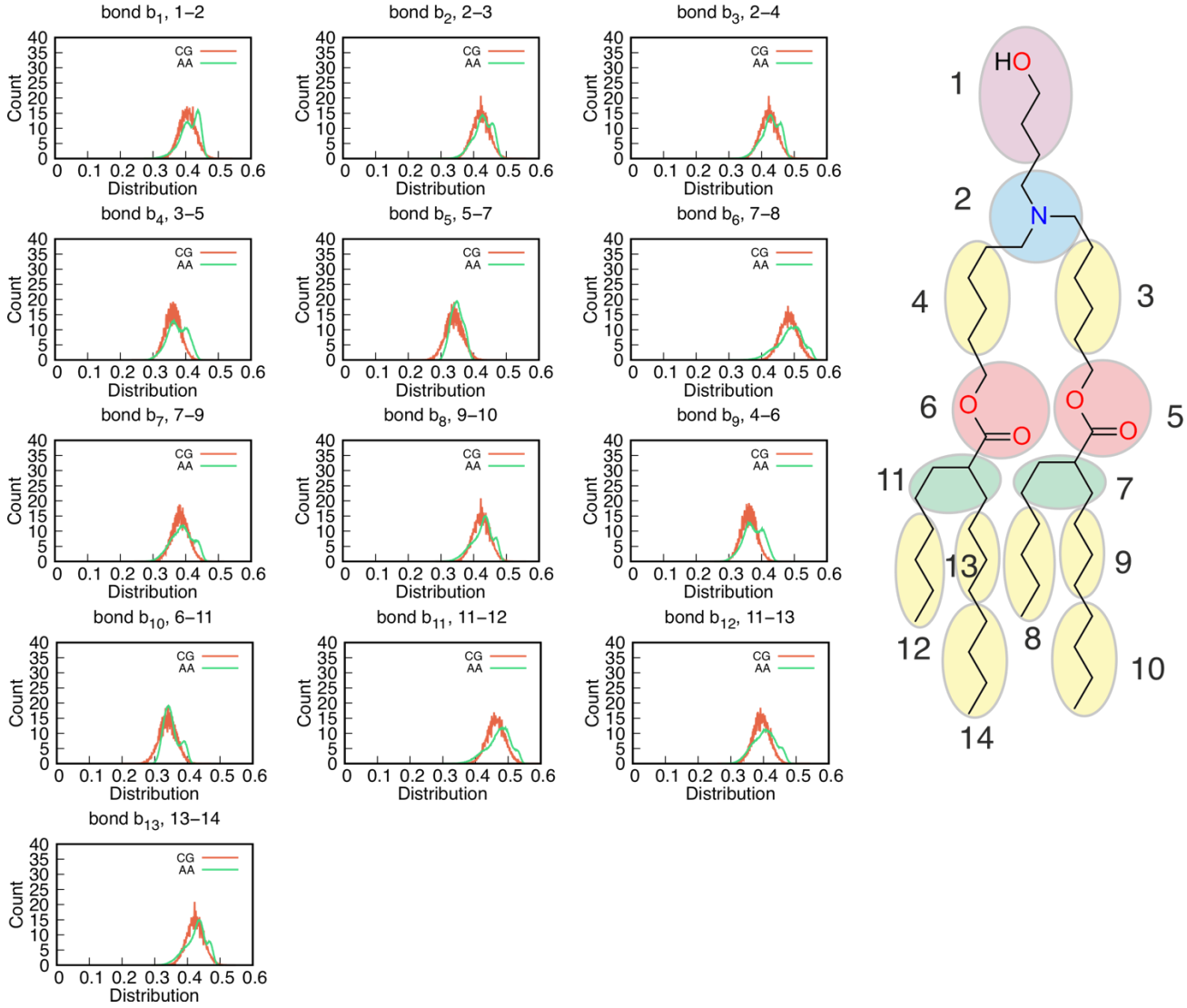

Figure S4. *The distributions of bond parameters extracted from all-atom (AA) and coarse grained (CG) simulations for ALC-0315 (neutral) lipid.*

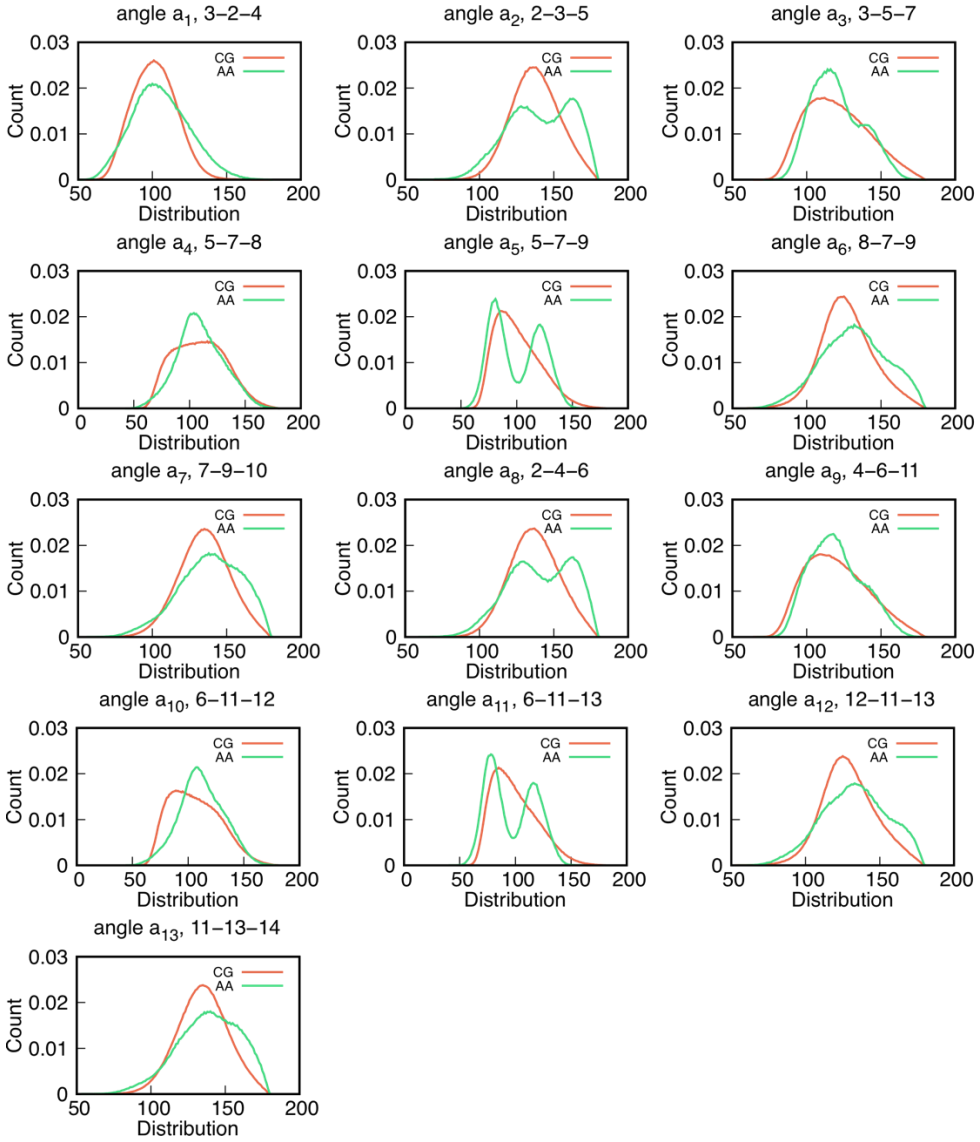

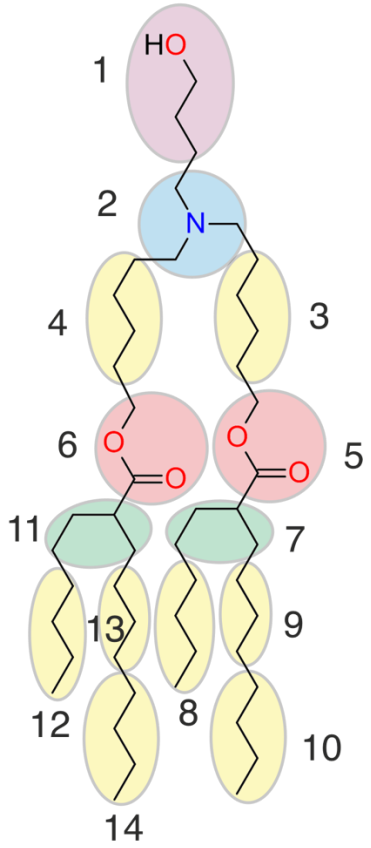

Figure S5. *The distributions of angle parameters extracted from all-atom (AA) and coarse grained (CG) simulations for ALC-0315 (neutral) lipid.*

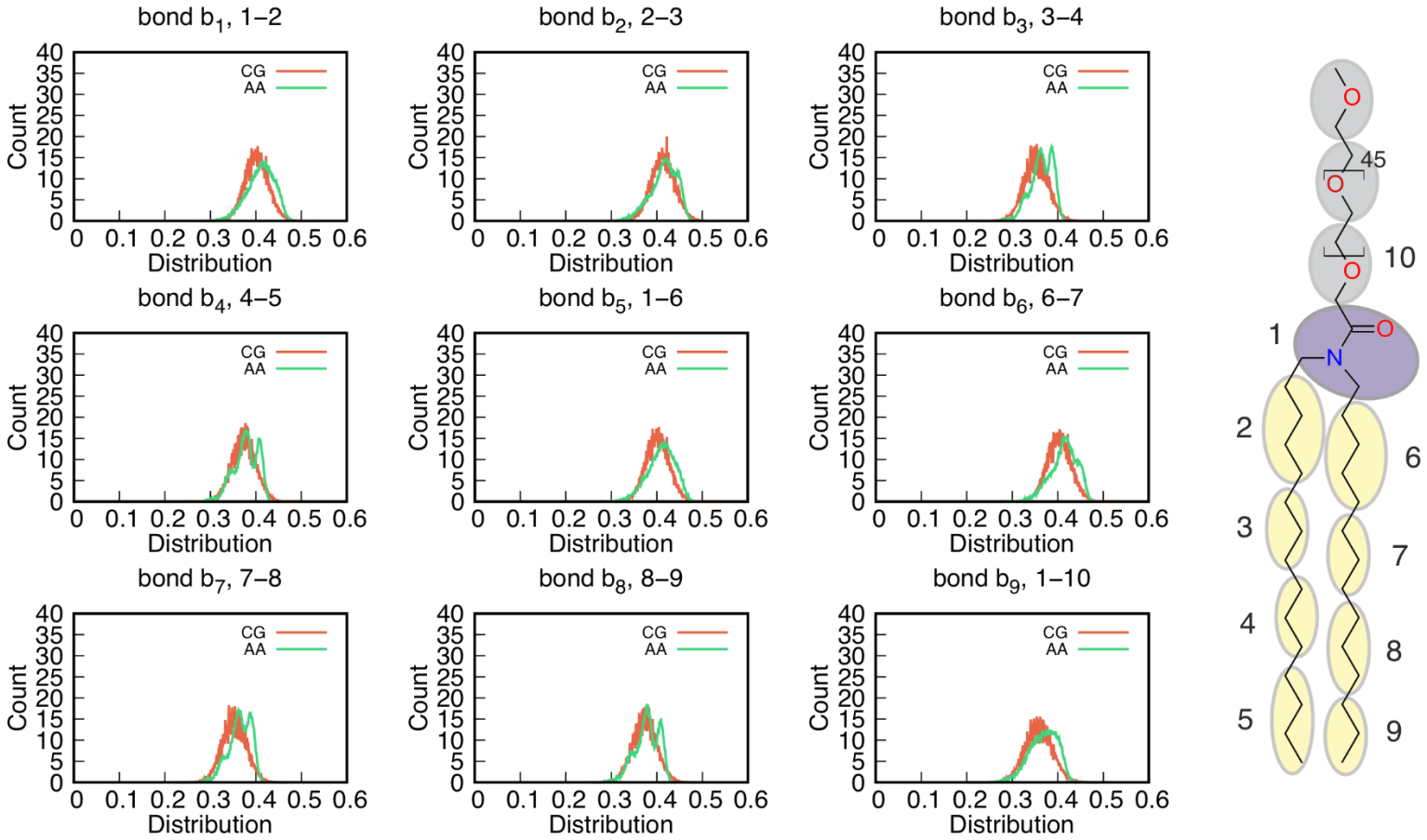

Figure S6. *The distributions of bond parameters extracted from all-atom (AA) and coarse grained (CG) simulations for ALC-0159 lipid.*

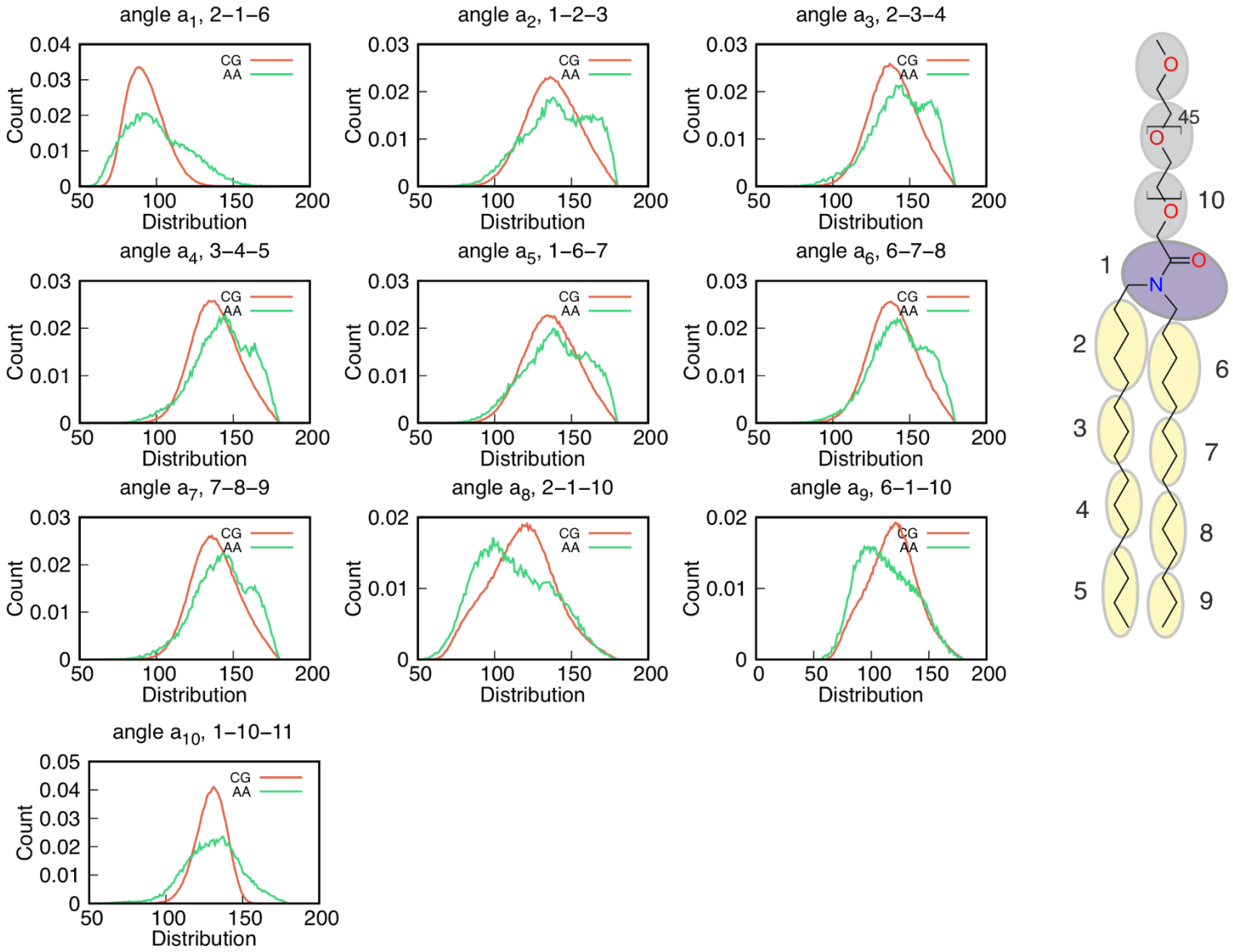

Figure S7. *The distributions of angle parameters extracted from all-atom (AA) and coarse grained (CG) simulations for ALC-0159..*

Furthermore, the area per lipid and membrane thickness were calculated and compared with the values of all atom simulation in our previous publication (ref 3). The bilayer thickness and area per lipid (Figure S8) in the presented models of charged ALC-0315 are shown in Table S1.

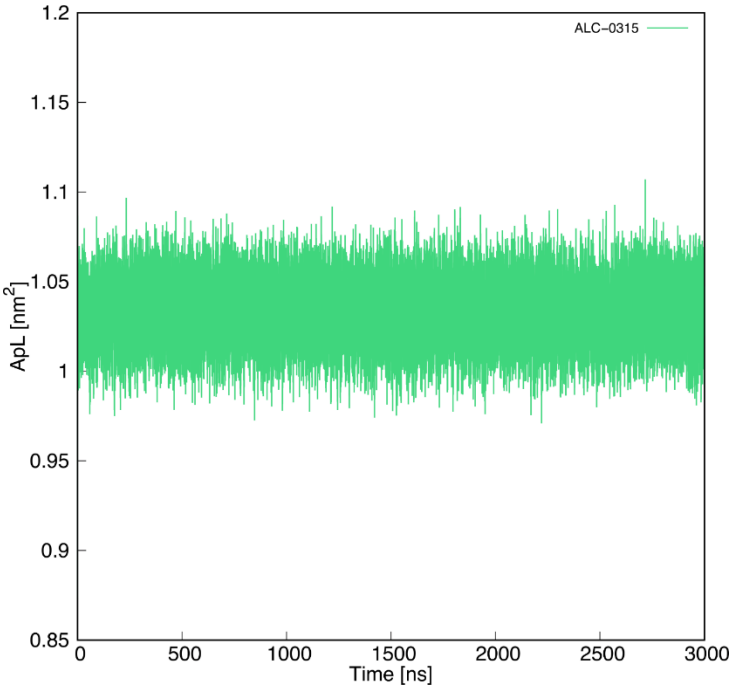

Figure S8. *Area per lipid (APL) for SM-102 (charged) and ALC-0315 (charged) CG membranes. The APL of the uncharged lipids was not calculated due to the bulk-like behavior of deprotonated lipids (see our previous publication)*

Table S1. *Area per Lipid (APL) and Head-to-Head membrane thickness (D_{HH}) for ALC-0315 (charged) CG membrane. D_{HH} was measured from the mass density profiles as the distance between peak maxima of N3a type bead densities of ILs. APL was calculated from the last 1 μs of CG simulation.*

System	APL [nm^2]	D_{HH} [nm]
ALC-0315 (charged)	1.032 ± 0.014	2.45

RNA parametrization

The topology for RNA was based on a version of polyU chain (decamer) kindly provided to us by S. Marrink and based on a beta version of MARTINI 3, which was used in ref. [5]. We adjusted the topology for MARTINI 3[1] – the parameters for the uracil base were taken from the published MARTINI 3 repository, while the bonded parameters for the backbone were taken from the model obtained from S. Marrink and the bead types for backbone were chosen based on the description of bead types in MARTINI 3. After preliminary simulations with bead types Q1, SN1a and SP1 (oRNA-*, see Table S2), we performed a potential of mean force (PMF) calculation of the U-tetramer in all-atom and coarse-grained resolution (*Figure S10*) and then adjusted the backbone beads to Q5, SN3a and SP1 (*Figure S9*).

The PMF calculations were based on weighted histogram analysis method (WHAM) using umbrella sampling on lipid bilayer composed of pure IL (or a layer of deprotonated IL) and a tetramer of RNA (tetraU chain). We prepared a model of tetraU in AA resolution (the Amber ff99SB[6] force field with the OL3[7] and parmbsc0[8] refinements for RNA and modified vdW radii for phosphate oxygens proposed

by Steinbrecher et al.[9]) and in CG resolution (varying bead types, see Figures S9 and S10) and performed 50 ns of unbiased simulation. Further, we pulled RNA molecule slowly inside lipid bilayer with a rate of 0.0001 nm per ns. We extracted starting snapshots for umbrella sampling simulations, based on the distances between RNA and lipid center of masses (separated by 0.2 nm from each other). Finally, we performed umbrella sampling simulations with a potential of 1,000 kJ mol^{-1} nm^{-1}. The umbrella sampling was performed for 50 ns (ALC-0315(0), AA), 100 ns (ALC-0315 (+1), AA and CG), and 200 ns (ALC-0315(0), CG) per window till the free energy profiles reached equilibrium.

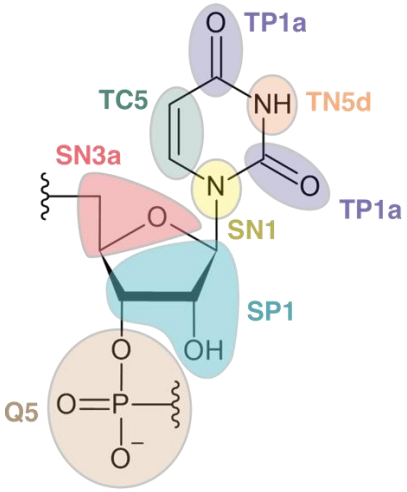

Figure S9. *Atomistic to coarse grained mapping scheme for the uracil monomeric unit.*

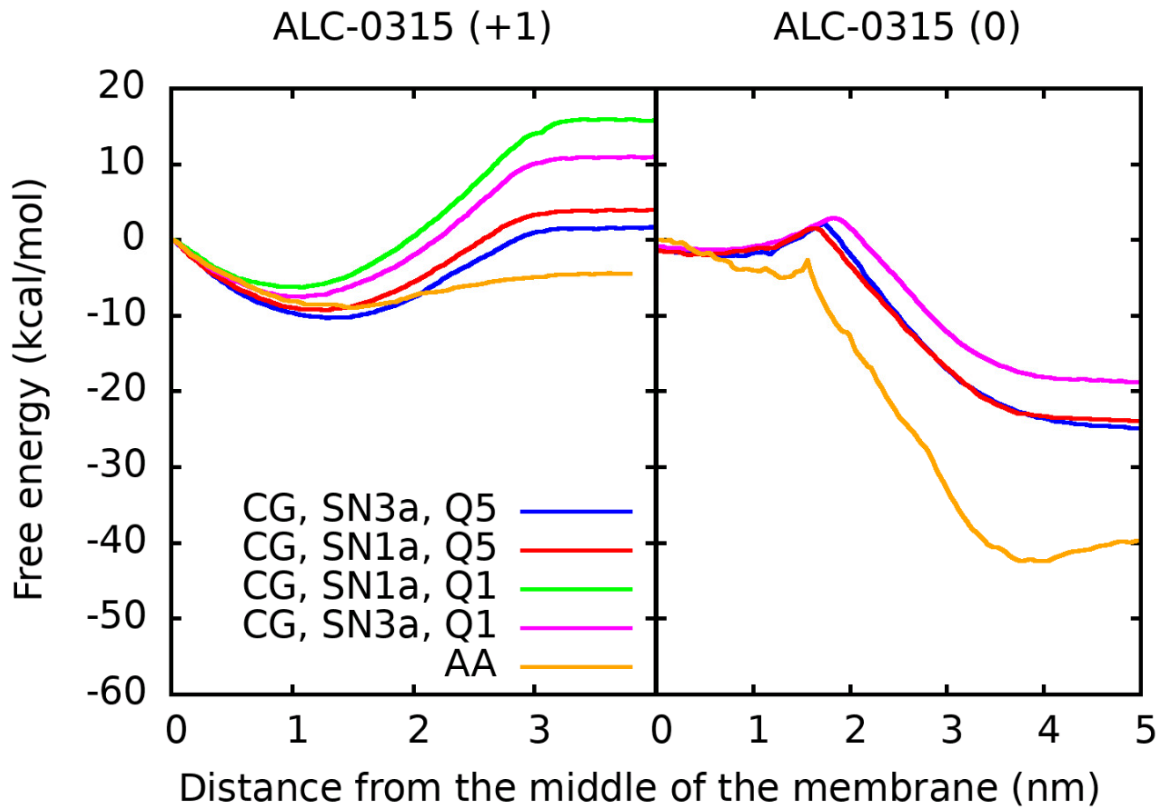

Figure S10: *Free energy profiles of tetrauracil chain with different bead combinations, on protonated bilayer (left) and deprotonated layer of ALC-0315 (IL).*

The potential of mean force simulations evaluate the free energy of a molecule in a given distance from the membrane center, leading to a calculated free energy profile (Fig. S10). Comparing different CG parametrizations with the AA profile can therefore evaluate, how well the CG system properties correspond to the AA ones. In the system containing the uncharged ionizable lipid (Fig. S10, right), the SN3a+Q5 and SN1a+Q5 RNA beadings behave in the same fashion and are more similar to the all-atom profile than the SN1a+Q1 beading. However, in the system containing the charged ionizable lipid (Fig. S10, left), the profile of the SN1a+Q5 beading matches the all-atom one more closely, leading to the ultimate decision to select this beading as the final parameters. It should be noted, that the most important principles are preserved in all studied models – in ILs, RNA preferential position is in the area of lipid head groups, while in the case of uncharged IL, the water fraction is preferred over the lipid fraction. We are aware of a missing local energy minimum in CG models near lipid head groups, which is common in CG membrane models.

MD simulations

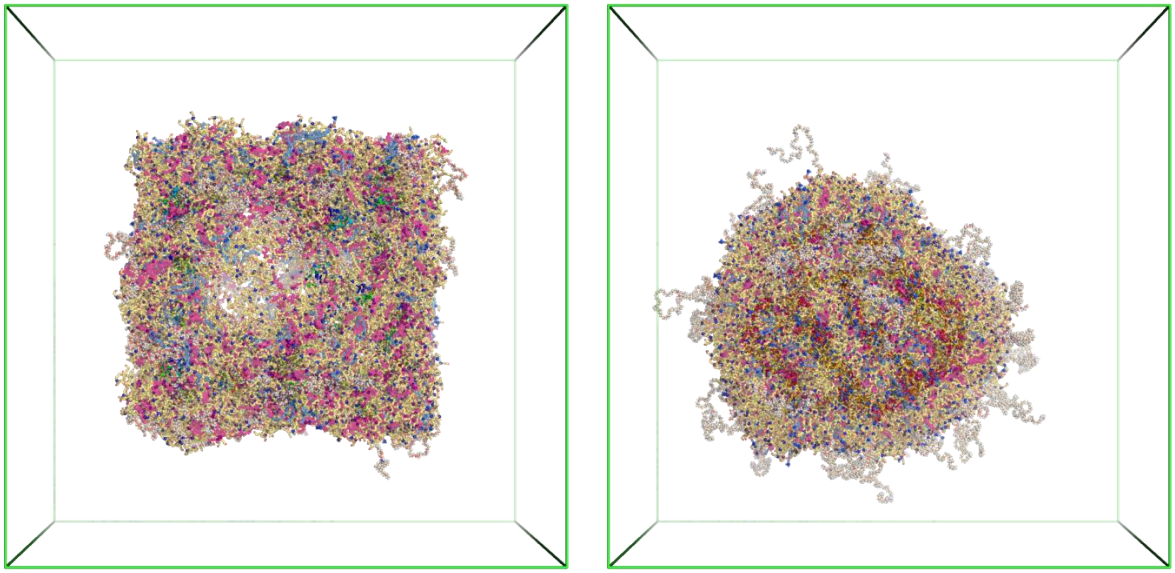

Figure S11*: Initial conformation (left) of lipids and RNA randomly inserted in a cubic box and the final conformation of LNP (right). Simulation boxes (green) are filled with water and ions, which are omitted for clarity. ILs are displayed in yellow, cholesterol in magenta, DSPC in blue and PEGylated lipids in orange. RNA is displayed in green cartoon.*

Analyses

Simulations were analyzed by home-made scripts using MD Analysis[10] and Lipyphilic[11] packages. We analyzed radial mass densities with respect to the LNP center of mass, radii of gyration of lipids (excluding PEGylated lipids), the amount of water beads inside LNP, and the number of contacts and contact enrichment between lipid head groups and between individual molecular types in the system. The analyses were performed throughout the simulation and either we report their evolution, or the last fifth of the simulation was taken for an average value. The last fifth of the simulation (1 μs in charged systems, 2 μs in uncharged systems and 400 ns in recharged simulations were already a stable system without further evolution for majority of the systems (except for noRNA-PEG-2000, noRNA-PEG-4000, noRNA-noPEG-4000, see Table S2 for system abbreviations). This decision was based on monitoring of the level of hydration (Figure S17). The PEG-covered LNP surface area was analyzed by the Voro++ software[12] facilitated by the trjVoronoi analysis tool.[13]

Below, a description of the individual analyses follows; the precise analysis workflow can be found in the attached python script. A sample script of the Voronoi analysis can be found in the dataset of our previous publication (doi.org/10.5281/zenodo.5595675).

- *Definition of LNP surface* – The simulation box was divided into 3D bins of x and y sides of 0.5 nm. The positions of lipid beads (except PEGylated lipids) were sorted out and the lowest and highest bead in z-direction was taken as the LNP surface.
- *Radius* - Average distance of surface beads from the center of mass.
- *Radius of gyration (R_g)* - Radius of gyration of all lipid species was calculated (without water and RNA).
- *Surface area* - LNP (lipids without PEGylated lipid and internal water) was analyzed by Alpha Shape 3D and the surface points were triangulated.
- *Hull2Sphere* - Ratio between the surface area of ideal sphere embedding the whole LNP and the real LNP surface area.
- *LNP hydration* - For each bin in z-axis, the water beads between the LNP surface beads were considered. The entire analysis was repeated along the x-axis, counting only water beads in both sets of "internal water" (to avoid artifacts at LNP edges). The amount of water beads was then recalculated per number of lipids in LNP.
- *PEG-covered LNP surface area (abbreviated as "PEG")* - The LNP surface and the surrounding layer of beads was extracted, and the contact area between surface beads and a) water, b) ions, c) all lipids and d) PEG was calculated. We report the fraction of PEG contacts to the total outer surface area (area in contact with non-lipid parts of the system), averaged over all beads and all selected frames.
- *Lipids enrichment* - Clustering of lipids was based on the analysis implemented[14] in LiPyphilic. The lipid headgroups within 0.7 nm were considered as in contact.
- *IL-water contacts* - Number of water beads within 0.7 nm of any IL bead (per lipid), calculated by LiPyphilic's 'Neighbours' tool
- *Radial density profile* - Density profile was calculated with respect to the center of mass of non-PEGylated lipids. Interspheres with thickness of 0.2 nm were constructed and for each of them the mass of individual parts of the system were calculated, divided by the volume of the respective intersphere.

***Table S2**: Overview of all performed simulations including compositions of used systems and simulation lengths*

	Number of molecules in the system								Simulation length (μs)		
System[&]	RNA-10 U	ALC-0315	ALC-0159	CHOL	DSPC	Na^+	Cl^-	W*	Charged	Uncharged	Recharged
RNA-PEG-1000	12	500	20	380	100	56	424	63 162	5	10	2
RNA-PEG-2000	25	1 000	40	760	200	113	838	126 386	5	10	2
RNA-PEG-4000	50	2 000	60	1 540	400	226	1 676	252 773	5	10	2
50RNA-PEG-4000	10x50-mer	2 000	60	1 540	400	147	1647	211029	5	10	2
200RNA-PEG-4000	2x200-mer	2 000	60	1 540	400	174	1774	249777	5	10	2
500RNA-PEG-4000	1x500-mer	2 000	60	1 540	400	174	1674	249714	5	10	2
oRNA-PEG-1000	12	500	20	380	100	56	424	63 162	5	10	2
oRNA-PEG-2000	25	1 000	40	760	200	113	838	126 386	5	10	2
oRNA-PEG-4000	50	2 000	60	1 540	400	226	1 676	252 773	5	10	2
noRNA-PEG-1000	-	500	20	380	100	43	543	62 414	10	10	2
noRNA-PEG-2000	-	1 000	40	760	200	86	1 086	123 422	5	10	2
noRNA-PEG-4000	-	2 000	60	1 540	400	147	2 147	211 517	5	10	2
oRNA-noPEG-1000	12	500	-	380	100	55	423	61 914	5**	10**	2
oRNA-noPEG-2000	25	1 000	-	760	200	111	836	123 890	5**	10**	2
oRNA-noPEG-4000	50	2 000	-	1 540	400	223	1 673	249 029	5**	10**	2
noRNA-noPEG-1000	-	500	-	380	100	43	543	61 164	5	10**	2
noRNA-noPEG-2000	-	1 000	-	760	200	85	1085	122 330	5	10**	2
noRNA-noPEG-4000	-	2 000	-	1 540	400	171	2 171	245 908	5	12**	2

*Number of water beads is shown, a water bead corresponds to four water molecules

**80 ns annealing period

[&]RNA stands for models with backbone bead types Q5, SN3a and SP1, oRNA stands for models with backbone bead types Q1, SN1a and SP1

Results

Global structural parameters

Here, the systems are described by their various features (see section Analyses for a precise description of all performed analyses), following the workflow of runs with charged, uncharged and recharged ILs.

Charged systems

***Table S3**: Structural parameters of charged LNPs, calculated from the last 1 μs of each simulation*

	Radius	R_g	Surface area	Hull2Sphere	LNP Hydration	PEG	DSPC-DSPC	IL-IL	IL-water
System	nm*	nm	nm^2		%	Surf%	Enrichment		#contacts[#]
RNA-PEG-1000	6.28±0.11	5.49±0.12	611.38±27.57	0.67±0.03	2.95±0.22	3.0	1.08±0.29	0.93±0.04	9.64±0.14
RNA-PEG-2000	7.97±0.12	6.89±0.13	989.13±46.06	0.69±0.05	4.79±0.18	3.5	1.14±0.16	0.95±0.04	8.79±0.08
RNA-PEG-4000	10.29±0.18	8.65±0.15	1605.75±72.95	0.74±0.03	8.13±0.33	3.0	1.15±0.16	0.96±0.03	8.35±0.07
50RNA-PEG-4000	10.34±0.15	8.79±0.15	1634.57±73.09	0.69±0.02	10.21±0.12	2.8	1.09±0.16	0.96±0.04	8.49±0.06
200RNA-PEG-4000	10.72±0.17	8.97±0.16	1685.66±81.27	0.72±0.02	14.02±0.18	2.5	1.05±0.17	0.94±0.04	9.11±0.06
500RNA-PEG-4000	10.42±0.16	8.80±0.16	1672.64±81.87	0.73±0.03	9.75±0.14	2.6	1.09±0.17	0.96±0.04	8.63±0.06
oRNA-PEG-1000	6.27±0.11	5.41±0.11	606.73±26.62	0.71±0.04	3.31±0.31	2.8	1.34±0.32	0.97±0.04	9.20±0.14
oRNA-PEG-2000	8.13±0.17	7.02±0.15	1013.63±51.70	0.66±0.04	4.82±0.21	2.9	1.21±0.19	0.98±0.04	8.52±0.08
oRNA-PEG-4000	10.38±0.19	8.78±0.18	1624.03±79.27	0.69±0.03	8.86±0.22	2.6	1.18±0.16	0.99±0.04	7.92±0.06
noRNA-PEG-1000	6.51±0.11	5.77±0.12	641.53±28.67	0.79±0.06	15.66±0.20	2.4	0.78±0.27	0.81±0.05	11.98±0.16
noRNA-PEG-2000	8.58±0.24	7.70±0.22	1109.88±60.32	0.67±0.05	19.21±0.33	2.4	0.90±0.24	0.83±0.04	11.60±0.13
noRNA-PEG-4000	11.18±0.24	9.53±0.21	1817.19±92.06	0.73±0.04	23.64±0.46	2.0	0.80±0.18	0.84±0.04	11.23±0.10
oRNA-noPEG-1000	6.22±0.08	5.15±0.07	598.68±19.46	0.73±0.03	3.25±0.23	-	1.36±0.31	0.93±0.04	9.59±0.12
oRNA-noPEG-2000	8.14±0.12	6.75±0.11	995.24±36.50	0.67±0.03	6.32±0.23	-	1.22±0.20	0.97±0.03	8.74±0.08
oRNA-noPEG-4000	10.20±0.12	8.54±0.14	1615.59±60.87	0.70±0.04	8.51±0.13	-	1.07±0.15	0.98±0.03	8.11±0.06
noRNA-noPEG-1000	6.46±0.15	5.60±0.18	634.82±33.30	0.65±0.06	13.06±0.20	-	0.75±0.28	0.82±0.05	12.02±0.14
noRNA-noPEG-2000	8.26±0.15	7.02±0.15	1039.91±54.43	0.73±0.04	16.09±0.27	-	0.89±0.22	0.84±0.04	11.50±0.10
noRNA-noPEG-4000	10.69±0.22	9.30±0.27	1760.10±101.12	0.64±0.04	16.73±0.17	-	0.94±0.18	0.85±0.03	11.04±0.14

*Average distance of surface beads from the center of mass [#]per residuum

***Table S4**: Number of contacts of RNA (per base) in charged LNPs with individual groups (calculated in CG resolution) and number of hydrogen bonds (calculated in AA resolution), calculated from the last 1 μs of each simulation*

	CG resolution						AA resolution		
System	RNA-IL	RNA-DSPC	RNA-CHOL	RNA-Na^+	RNA-Cl^-	RNA-WAT	Hbonds RNA-IL	Hbonds RNA-CHOL	Hbonds RNA-RNA
RNA-PEG-1000	4.58±0.12	1.45±0.09	1.19±0.16	0.00±0.00	1.79±0.13	3.70±0.24	0.68±0.04	0.17±0.02	0.62±0.02
RNA-PEG-2000	4.66±0.10	1.26±0.06	1.14±0.15	0.04±0.01	1.93±0.12	3.88±0.25	0.71±0.03	0.21±0.01	0.48±0.03
RNA-PEG-4000	4.74±0.08	1.25±0.06	1.09±0.13	0.02±0.00	1.97±0.09	4.05±0.20	0.70±0.01	0.16±0.01	0.52±0.02
50RNA-PEG-4000	4.90±0.06	0.90±0.03	1.06±0.12	0.24±0.02	1.88±0.09	3.58±0.18	0.74±0.01	0.17±0.01	0.36±0.01
200RNA-PEG-4000	4.87±0.07	0.88±0.04	1.08±0.13	0.31±0.02	1.86±0.10	3.66±0.19	0.79±0.03	0.18±0.01	0.36±0.02
500RNA-PEG-4000	4.71±0.06	1.06±0.03	1.03±0.13	0.35±0.01	1.83±0.07	3.61±0.19	0.70±0.02	0.19±0.01	0.38±0.01
oRNA-PEG-1000	5.28±0.11	0.87±0.09	0.96±0.15	0.00±0.00	1.69±0.13	1.14±0.21	0.87±0.05	0.14±0.02	0.63±0.04
oRNA-PEG-2000	5.25±0.07	0.94±0.05	1.01±0.16	0.00±0.00	1.69±0.09	1.44±0.16	0.86±0.02	0.19±0.02	0.64±0.02
oRNA-PEG-4000	5.41±0.07	0.86±0.05	0.98±0.12	0.00±0.00	2.02±0.09	1.74±0.13	0.84±0.02	0.22±0.02	0.60±0.01
oRNA-noPEG-1000	4.94±0.15	1.09±0.09	1.04±0.14	0.00±0.00	1.50±0.11	1.23±0.19	0.78±0.05	0.22±0.01	0.62±0.03
oRNA-noPEG-2000	5.24±0.09	0.99±0.04	1.00±0.11	0.00±0.00	1.78±0.08	1.44±0.15	0.88±0.03	0.14±0.01	0.63±0.02
oRNA-noPEG-4000	5.36±0.06	0.89±0.04	0.97±0.09	0.02±0.00	1.99±0.07	1.57±0.15	0.83±0.02	0.17±0.01	0.60±0.01

Uncharged systems

***Table S5**: Structural parameters of uncharged LNPs, calculated from the last 2 μs of each simulation*

	Radius	R_g	Surface area	Hull2Sphere	LNP Hydration	PEG	RNA	DSPC-DSPC	IL-IL	IL-water
System	nm*	nm	nm^2		%	Surf%	[&]	Enrichment		#contacts
RNA-PEG-1000	6.10±0.08	5.15±0.08	559.52±23.42	0.80±0.03	1.38±0.16	4.2	16.61±0.26	2.36±0.43	1.12±0.04	5.98±0.41
RNA-PEG-2000	7.72±0.10	6.43±0.10	889.36±33.95	0.84±0.02	1.44±0.14	5.3	11.98±0.10	2.99±0.42	1.16±0.03	4.47±0.29
RNA-PEG-4000	9.83±0.13	7.98±0.11	1416.79±54.82	0.85±0.02	2.21±0.10	4.6	7.95±0.13	3.06±0.39	1.17±0.02	3.63±0.23
50RNA-PEG-4000	9.81±0.13	7.97±0.11	1410.76±53.74	0.86±0.02	1.99±0.11	4.5	0.00±0.00	3.76±0.46	1.19±0.02	3.54±0.24
200RNA-PEG-4000	9.77±0.13	7.94±0.11	1405.93±52.88	0.86±0.02	1.43±0.09	4.9	0.00±0.00	3.98±0.45	1.20±0.02	3.31±0.22
500RNA-PEG-4000	9.79±0.13	7.96±0.11	1413.64±54.64	0.86±0.02	1.85±0.11	4.6	0.00±0.00	3.20±0.39	1.20±0.02	3.29±0.23
oRNA-PEG-1000	6.09±0.08	5.13±0.08	559.81±23.68	0.81±0.02	1.21±0.13	4.3	8.32±0.12	2.92±0.46	1.14±0.04	5.80±0.41
oRNA-PEG-2000	7.71±0.10	6.40±0.10	889.40±35.56	0.81±0.10	1.29±0.10	5.3	0.00±0.00	2.91±0.38	1.17±0.03	4.27±0.30
oRNA-PEG-4000	9.82±0.13	7.98±0.11	1414.89±54.31	0.86±0.03	2.11±0.13	4.4	8.09±0.13	3.15±0.39	1.17±0.02	3.58±0.24
noRNA-PEG-1000	6.11±0.08	5.14±0.08	561.18±23.25	0.81±0.02	1.95±0.21	3.6	-	3.43±0.52	1.12±0.04	6.33±0.40
noRNA-PEG-2000	7.81±0.10	6.47±0.09	898.80±35.15	0.84±0.02	3.44±0.15	4.1	-	3.92±0.44	1.16±0.03	5.21±0.31
noRNA-PEG-4000	10.02±0.14	8.16±0.11	1450.66±55.73	0.83±0.02	5.86±0.39	3.7	-	3.53±0.43	1.17±0.02	4.42±0.26
oRNA-noPEG-1000	7.69±0.07	6.12±0.06	876.31±25.24	0.84±0.02	1.18±0.11	-	8.00±0.12	3.28±0.36	1.14±0.03	4.67±0.23
oRNA-noPEG-2000	9.75±0.09	7.72±0.07	1391.82±38.86	0.86±0.02	1.65±0.09	-	5.98±0.06	3.57±0.36	1.16±0.02	3.71±0.19
oRNA-noPEG-4000	6.06±0.06	4.87±0.05	551.27±17.16	0.81±0.03	1.19±0.15	-	8.34±0.02	3.11±0.45	1.12±0.04	6.16±0.31
noRNA-noPEG-1000	6.06±0.06	4.88±0.05	550.28±15.71	0.81±0.02	1.51±0.15	-	-	3.63±0.49	1.11±0.03	6.31±0.32
noRNA-noPEG-2000	7.70±0.08	6.14±0.06	874.56±25.00	0.84±0.02	1.84±0.10	-	-	4.37±0.46	1.13±0.03	5.12±0.26
noRNA-noPEG-4000	9.77±0.09	7.75±0.07	1388.41±38.05	0.86±0.02	2.33±0.11	-	-	4.68±0.36	1.16±0.02	4.10±0.18

*Average distance of surface beads from center of mass [#]per residuum [&]% remaining inside LNP

***Table S6**: Number of contact of RNA (per base) embedded in uncharged LNPs with individual groups calculated in CG resolution from the last 2 μs of each simulation*

System	RNA-IL	RNA-DSPC	RNA-CHOL	RNA-NA	RNA-CL	RNA-WAT
RNA-PEG-1000	2.72±0.41	3.79±0.24	1.22±0.35	5.17±0.14	0.41±0.10	7.40±0.34
RNA-PEG-2000	1.10±0.27	3.51±0.26	0.54±0.19	6.13±0.11	0.43±0.04	6.98±0.31
RNA-PEG-4000	1.66±0.22	3.53±0.21	0.83±0.21	6.31±0.09	0.32±0.05	7.00±0.19
50RNA-PEG-4000*	-	-	-	6.77±0.08	0.32±0.03	6.84±0.16
200RNA-PEG-4000*	-	-	-	6.69±0.10	0.35±0.04	7.01±0.17
500RNA-PEG-4000*	-	-	-	6.79±0.09	0.47±0.03	6.88±0.16
oRNA-PEG-1000	1.70±0.49	5.00±0.46	0.80±0.40	5.56±0.14	0.06±0.05	6.86±0.27
oRNA-PEG-2000	0.00±0.00	0.00±0.00	0.00±0.00	6.61±0.11	0.01±0.01	5.86±0.22
oRNA-PEG-4000	2.85±0.34	3.28±0.24	1.31±0.26	6.52±0.09	0.09±0.02	5.39±0.18
oRNA-noPEG-1000	2.05±0.33	4.80±0.39	1.08±0.29	6.22±0.09	0.15±0.02	5.87±0.19
oRNA-noPEG-2000	1.65±0.31	2.87±0.26	0.81±0.28	6.60±0.08	0.11±0.02	5.71±0.12
oRNA-noPEG-4000	2.12±0.49	5.25±0.47	1.07±0.44	5.61±0.13	0.04±0.04	7.06±0.24

*no RNA was preserved inside LNP

Recharged systems

***Table S7**: Structural parameters of charged LNPs, calculated from the last 400 ns of each simulation*

	Radius	R_g	Surface area	Hull2Sphere	LNP Hydration	DSPC-DSPC	IL-IL	IL-water
System	nm*	nm	nm^2		%	Enrichment		#contacts[#]
RNA-PEG-1000	6.35±0.11	5.72±0.12	635.63±26.89	0.62±0.04	4.39±0.18	0.92±0.27	0.88±0.05	10.41±0.17
RNA-PEG-2000@	9.52±0.18	8.65±0.16	1219.00±53.24	0.44±0.01	7.22±0.35	1.17±0.12	0.92±0.05	9.50±0.08
RNA-PEG-4000@	12.61±0.48	11.25±0.39	2056.84±106.41	0.48±0.02	10.30±0.49	1.08±0.20	0.95±0.04	9.16±0.05
50RNA-PEG-4000@	11.26±0.19	10.65±0.32	1984.58±92.11	0.50±0.01	11.15±0.13	1.28±0.18	0.95±0.04	9.10±0.04
200RNA-PEG-4000@	11.34±0.30	9.74±0.26	1890.62±105.27	0.48±0.01	13.10±0.23	1.13±0.18	0.93±0.04	9.64±0.08
500RNA-PEG-4000@	11.92±0.21	10.47±0.24	1986.46±92.62	0.46±0.01	13.55±0.41	1.07±0.20	0.94±0.04	9.42±0.07
oRNA-PEG-1000@	7.54±0.14	6.87±0.15	722.41±29.45	0.43±0.01	5.58±0.45	1.30±0.41	0.94±0.04	9.83±0.14
oRNA-PEG-2000@	9.16±0.25	8.03±0.23	1157.48±64.85	0.44±0.01	7.10±0.79	1.51±0.22	0.97±0.05	9.03±0.07
oRNA-PEG-4000	10.48±0.19	8.93±0.18	1669.57±84.19	0.65±0.03	9.84±0.19	1.38±0.25	0.97±0.04	8.66±0.06
noRNA-PEG-1000	6.41±0.13	5.67±0.14	629.39±31.42	0.69±0.04	10.64±0.19	1.44±0.26	0.81±0.05	11.85±0.11
noRNA-PEG-2000	8.35±0.16	7.16±0.14	1047.97±54.53	0.73±0.02	14.63±0.23	1.19±0.28	0.83±0.04	11.23±0.08
noRNA-PEG-4000	10.75±0.19	9.08±0.18	1741.91±90.00	0.77±0.03	18.91±0.28	1.30±0.20	0.85±0.04	11.03±0.10
oRNA-noPEG-1000	6.35±0.13	5.46±0.14	633.83±31.34	0.65±0.04	3.93±0.27	1.19±0.32	0.90±0.05	10.31±0.11
oRNA-noPEG-2000@	9.50±0.18	8.60±0.19	1217.25±61.82	0.44±0.01	7.39±1.31	1.45±0.26	0.95±0.05	9.50±0.10
oRNA-noPEG-4000	10.38±0.14	8.55±0.14	1651.13±78.61	0.76±0.03	10.71±0.37	2.28±0.20	0.98±0.05	9.07±0.06
noRNA-noPEG-1000	6.33±0.10	5.42±0.12	619.25±29.33	0.71±0.03	10.43±0.19	1.17±0.26	0.82±0.05	11.96±0.13
noRNA-noPEG-2000	8.68±0.36	7.36±0.23	1079.76±64.43	0.65±0.04	12.62±0.98	1.15±0.24	0.83±0.04	11.52±0.13
noRNA-noPEG-4000	10.46±0.16	8.66±0.15	1640.88±77.07	0.80±0.04	16.85±0.14	1.08±0.18	0.85±0.04	11.05±0.08

@Pbc error – a periodic tube was formed instead of LNP

Figures and plots

Radial densities

The total lipid radial density profiles of all systems (Fig. S12) and the per-lipid density of the RNA-PEG-4000 (Fig. S13), show the charge-dependent LNP homogeneity and inner water presence. The radial density profiles were calculated with respect to the center of mass of non-PEGylated lipids. Interspheres with thickness of 0.2 nm were constructed and for each of them the mass of individual parts of the system were calculated, divided by the volume of the respective intersphere. The radial densities correspond to the mass densities of the LNP, calculated from its center of mass outwards.

The lipid radial densities (Fig. S12) show marked difference in the LNP organization, based on the charge state of the ionizable lipid. In the charged (and recharged) simulations, the lipid density of the LNP is dependent on the position from the particle's center of mass, due to the presence of water- or RNA-filled spaces within. In the case of recharged simulations, some of the systems did not converge to LNP, but to periodic tubuli, therefore the radial averaging does not lead to homogenous profiles. The gradual decrease in the density profiles corresponds to irregularity of the particle shape. On the other hand, the plateau of lipid density with a sharp drop in the uncharged simulations corresponds to a dense, lipid filled spherical particle. The different positions of the density decrease show the size of the LNP based on the number of lipids in the system.

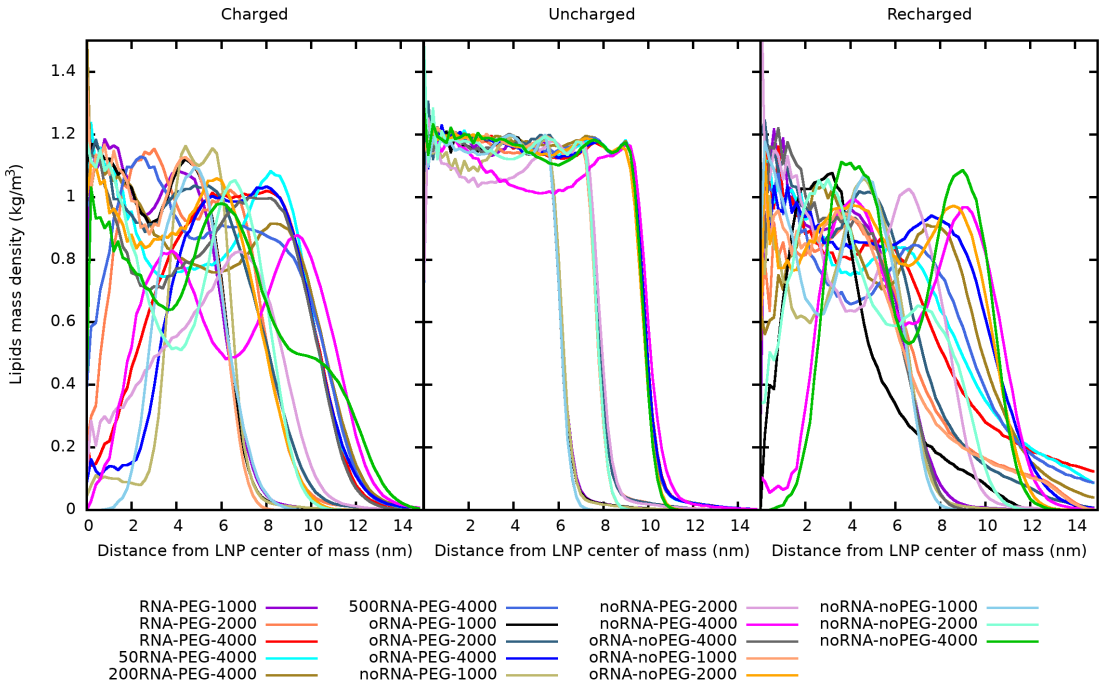

Figure S12: *Radial density profiles of non-PEGylated lipids (DSPC, ALC-3015, CHOL) for charged (left), uncharged (middle) and recharged (right) LNPs calculated for each simulation.*

The radial mass densities of different parts of a sample system (Fig. S13) depicts these differences in detail. The overall lipid density (red line) corresponds to the data shown in Figure S12, with green, brown, magenta, and cyan lines depicting the respective lipid components of the system.

In the charged system, with the IL in its protonated form, the mass of lipids (with the exception of the PEGylated ALC-0159) is spread in a broad peak with the maximum at around 6.0-8.0 nm from the LNP center, around a peak of water density, corresponding to a (PEG-containing) water bubble in the middle of the LNP. Although the water density decreases at 6.0-8.0 nm, it does not drop all the way to zero. This corresponds to other water bubbles and water surrounding RNA inside LNP. In contrast, in the uncharged system, with the IL in its deprotonated form, the densities of non-PEGylated lipids are more

homogeneous in their plateu-like shape from the center of the LNP to about 10.0 nm. While there is a small peak of (PEG and) water density at 4.0-8.0 nm from the center (corresponding to remaining water bubbles), the majority of water (and PEG) mass is located out of the LNP. The entire peak of RNA mass in the charged system is located in the lipid phase at around 4.0-8.0 nm, at the water density minimum. On the other hand, the RNA mass in the uncharged system is located both within the LNP and out of it. To compare the absolute values of densities, the reader is reminded that these are radial densities that do not scale linearly.

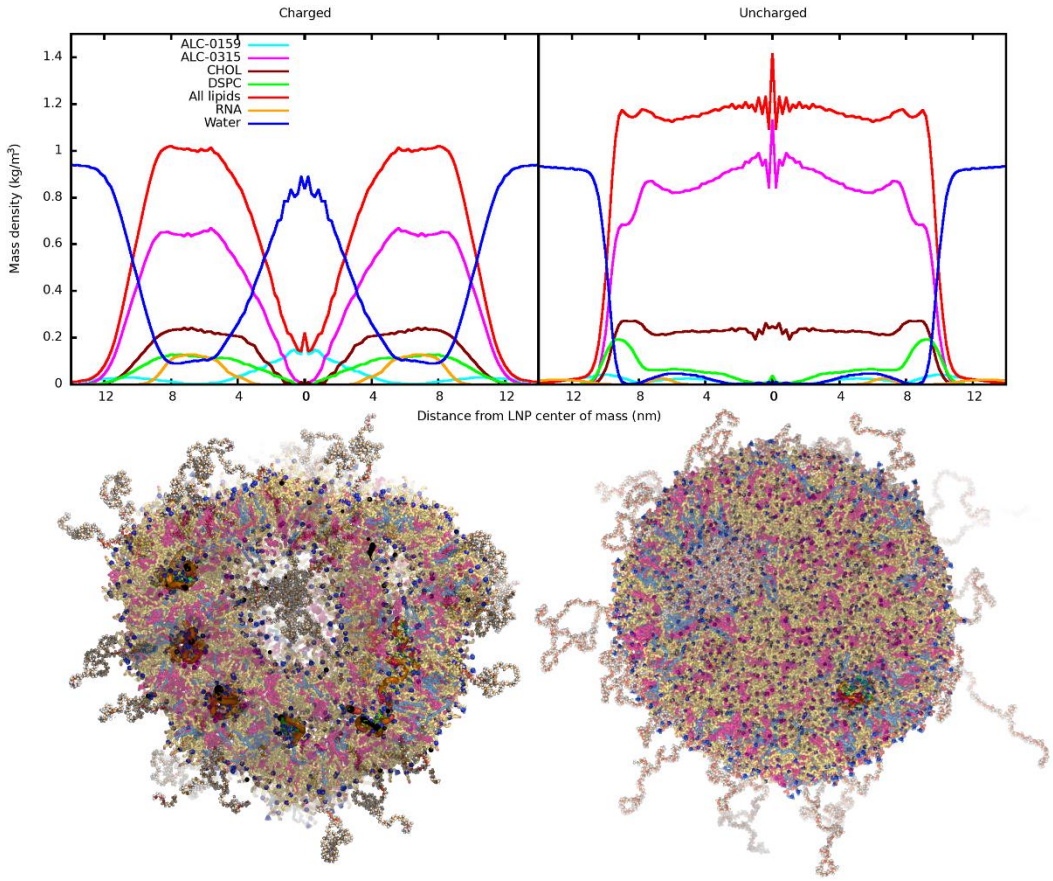

***Figure S13**: Radial density profiles of individual LNP components for LNP with 4000 lipids with RNA and PEG (RNA-PEG-4000, upper panel). For clarity, radial density profiles are shown twice with final structures of corresponding LNPs in corresponding scale (lower panel). ILs are displayed in yellow, cholesterol in magenta, DSPC in blue sticks and RNA as colored cartoon.*

LNP shape analyses

The overall LNP shape, in all its variations between systems, is challenging to describe using only one property. Tables S3 and S5 describe the differences in the shape and "roundness" of the LNP in the manner of the LNP radius, radius of gyration, surface area and the Hull2Sphere ratio (ratio between the LNP surface area and the surface area of a perfect sphere circumscribed LNP, Figure S14). The Figures S15 and S16 depict the time-dependent evolution of the surface area and radius of gyration calculated for the non-PEGylated lipids. The surface area was analyzed by Alpha Shape 3D and the surface points were triangulated. Both properties show stable LNP in charged state and a sudden decrease of surface area and radius of gyration after IL deprotonation. This corresponds to the more spherical shape of the LNPs. The further decrease in LNP size, therefore also its surface area and radius of gyration corresponds to a gradual dehydration of LNP (see further Figure S17).

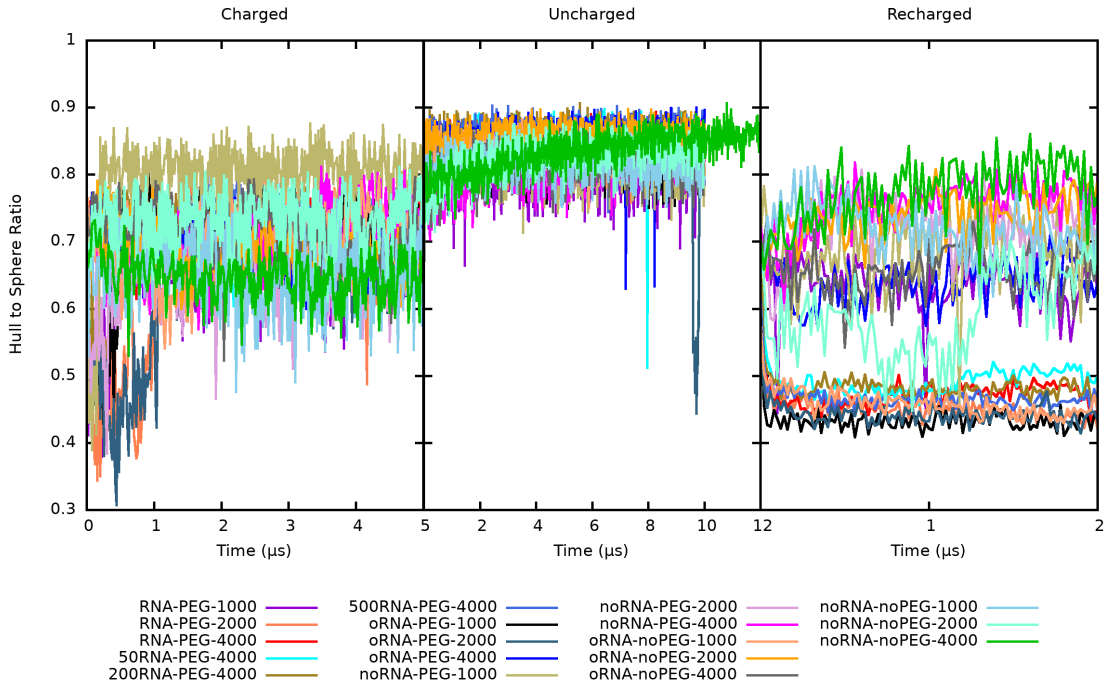

Figure S14: *Ratio of a surface area of a convex hull embedding LNP and a sphere circumscribed LNP. The higher value in case of uncharged LNPs show more spherical particles. The very low values in some of recharged LNPs correspond to the formation of periodic tubes.*

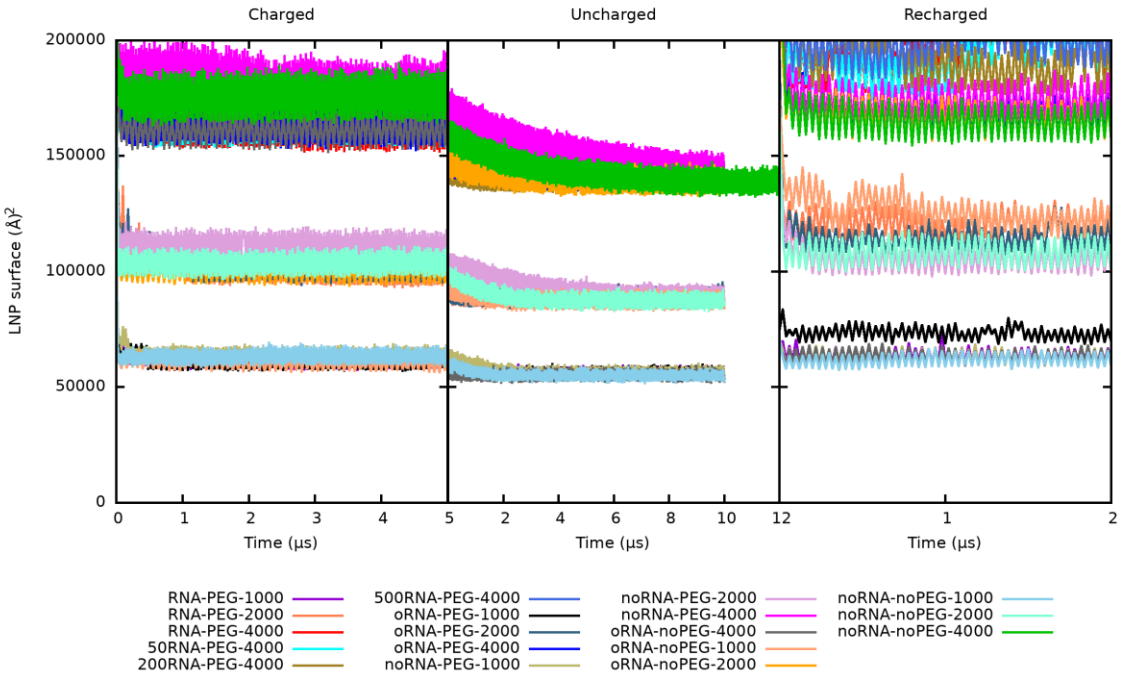

Figure S15*: LNP surface area (excluding PEGylated lipids) calculated for each simulation. Fluctuations of the LNP surface area corresponds to the effect of simulated annealing.*

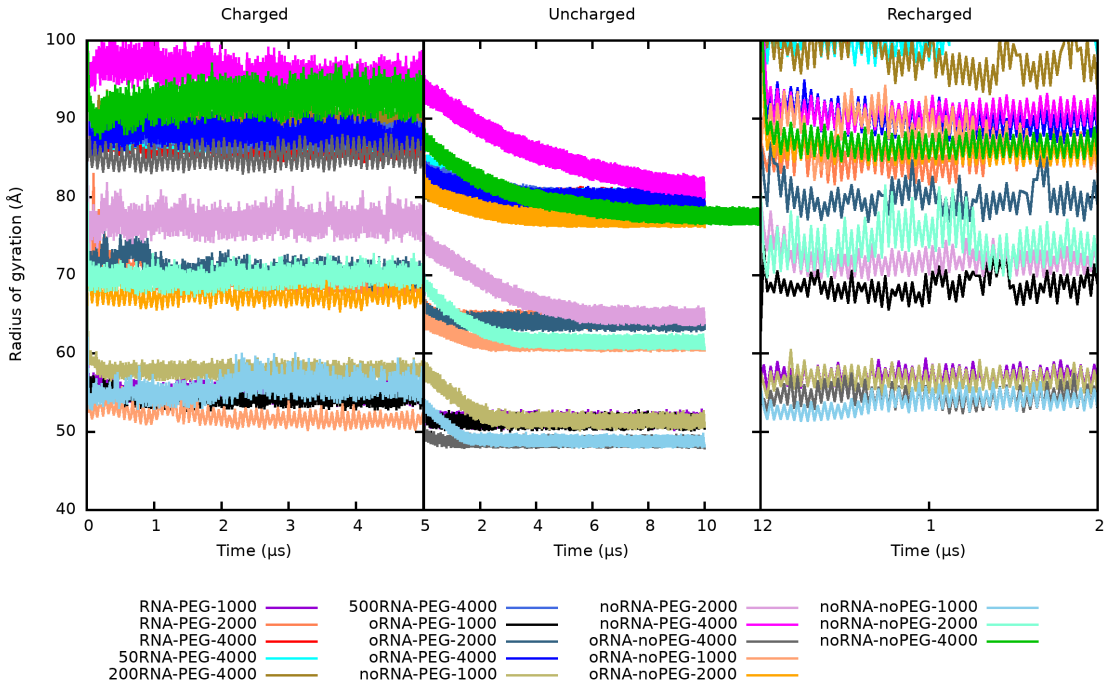

***Figure S16**: Radius of gyration of lipids (without PEG chains) in LNPs calculated for each simulation. Fluctuations of the radii of gyration corresponds to the effect of simulated annealing.*

Water and lipid Behavior

Based on IL charge, the LNPs change their water content (Fig. S17) and lipid mixing (Fig. S18) rapidly.

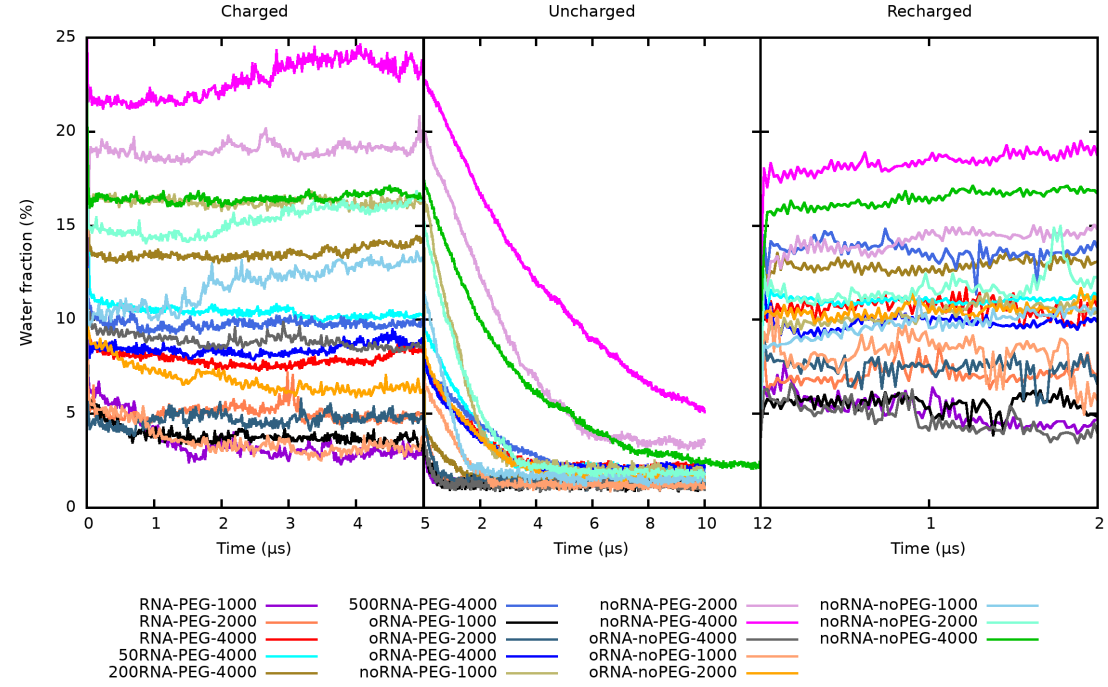

***Figure S17**: LNP level of hydration calculated for each simulation.*

The evolution of water content inside the LNP is depicted in Figure S17 as the fraction of LNP mass made by water located inside the particle. In the charged systems, the water content within the LNP is mostly dependent on the presence of RNA. The RNA-free LNPs contain a higher fraction of water than RNA-containing LNPs. Upon the charge change after IL deprotonation, the fraction of water inside the particle starts dropping rapidly, down to about 2% of the total water content. Similarly, the water content inside the particle rapidly increases after the reprotonation of the IL, although the water levels is affected by formation of periodic tubuli.

Lipid enrichment (Figure S18) is a property defined in Ingólfsson et al.,[14] which we calculated using the LiPyphilic analysis toolkit. Defined as a fraction of contacts of a given lipid around a reference lipid, out of average contact of the given lipid with all other lipids, it can be used to show the clustering of lipid species. The lipid headgroups within 0.7 nm were considered as in contact. In the charged systems, the enrichment of DSPC around DSPC fluctuates around, or slightly above 1 (see: Table S3), which corresponds to the average distribution of DSPC around DSPC compared to the rest of the system. In contrast, the enrichment values in the uncharged systems rise rapidly, showing that a DSPC molecule is more likely to be found around another DSPC than it is the average, therefore DSPC molecules are clustering together. After the reprotonation of ILs, DSPC mixes again with other lipids rapidly.

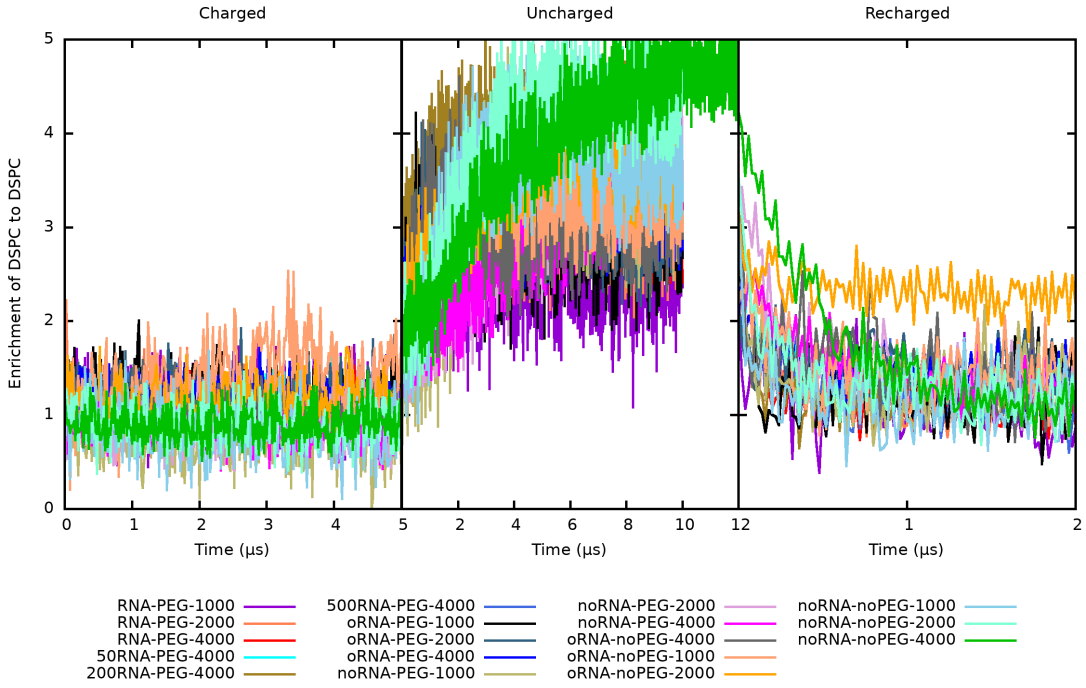

***Figure S18**: Density enrichment of DSPC around other DSPC molecules calculated for each simulation. In charged LNPs (left), DSPC stays in a random distribution, while in uncharged LNPs (middle), DSPC gradually clusters. After reprotonation of ILs, DSPC mixes again (right).*

RNA-lipid contacts

The RNA-lipid contacts were calculated for each of the non-PEGylated lipids in the charged (Fig. S19) and uncharged (Fig. S20) systems (see also tables S4 and S6).

In the charged systems (Figure S19), the RNA is mostly in contact (number of beads within 0.7 nm) with the ionizable lipid and less with DSPC and cholesterol. In contrast, in the uncharged systems (Figure S20) there is a marked increase in the RNA-DSPC contacts and decrease in the IL-RNA contacts.

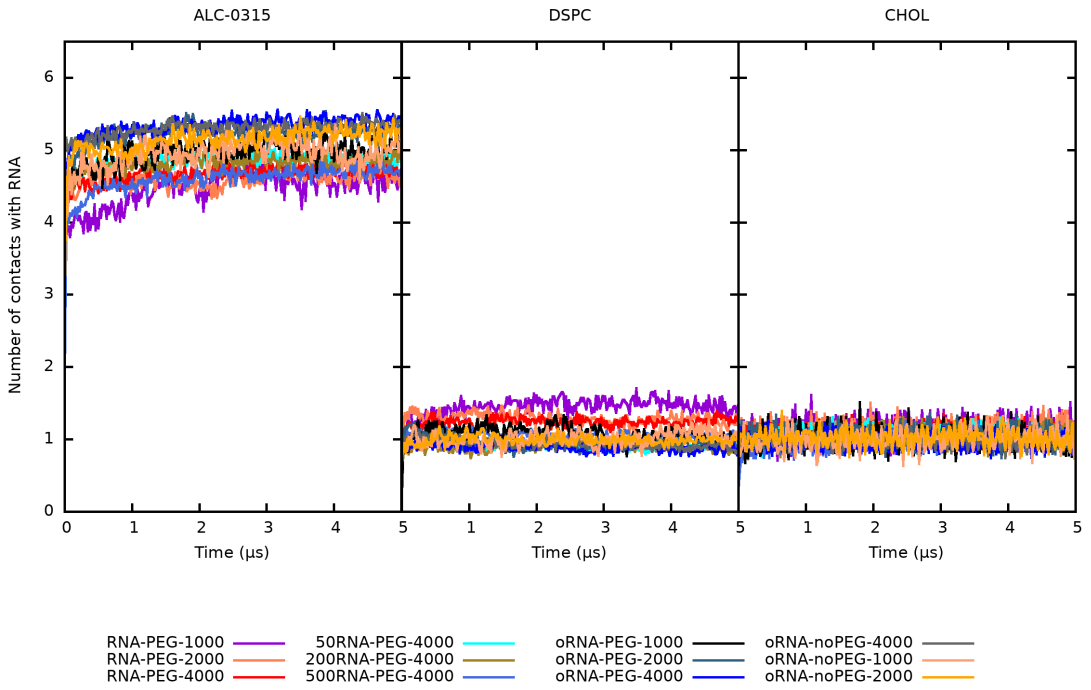

***Figure S19**: Number of contacts of each lipid with RNA in protonated LNP, calculated for each simulation.*

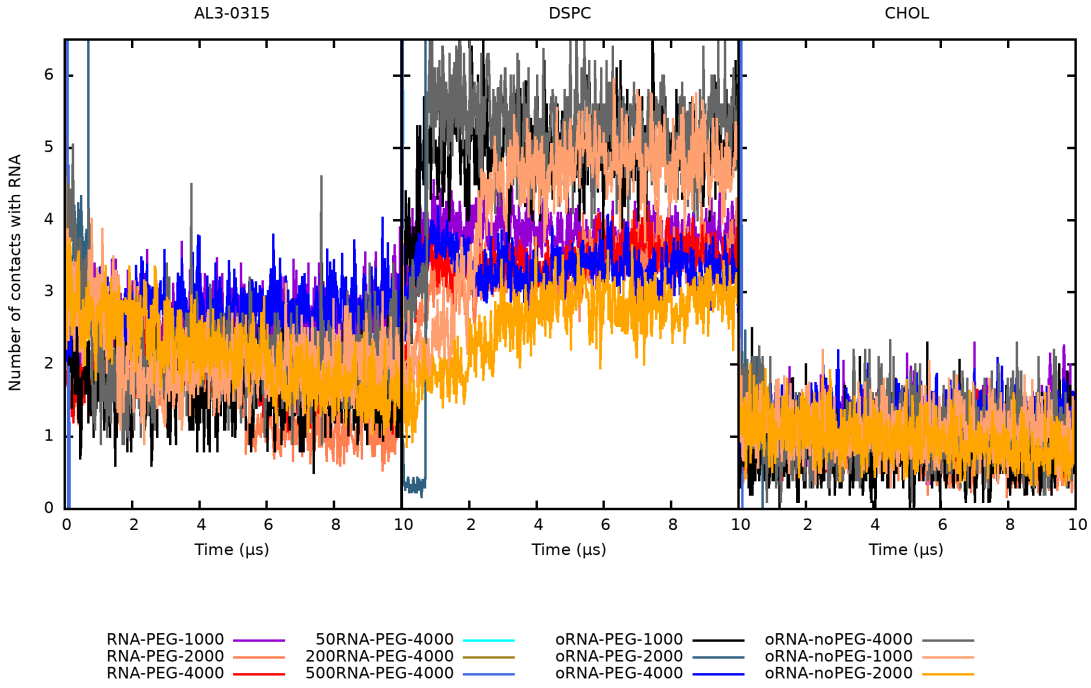

***Figure S20**: Number of contacts of each lipid with RNA remaining in deprotonated LNPs, calculated for each simulation.*

The difference in RNA-lipid binding can be also seen directly in the structures (Fig. S21).

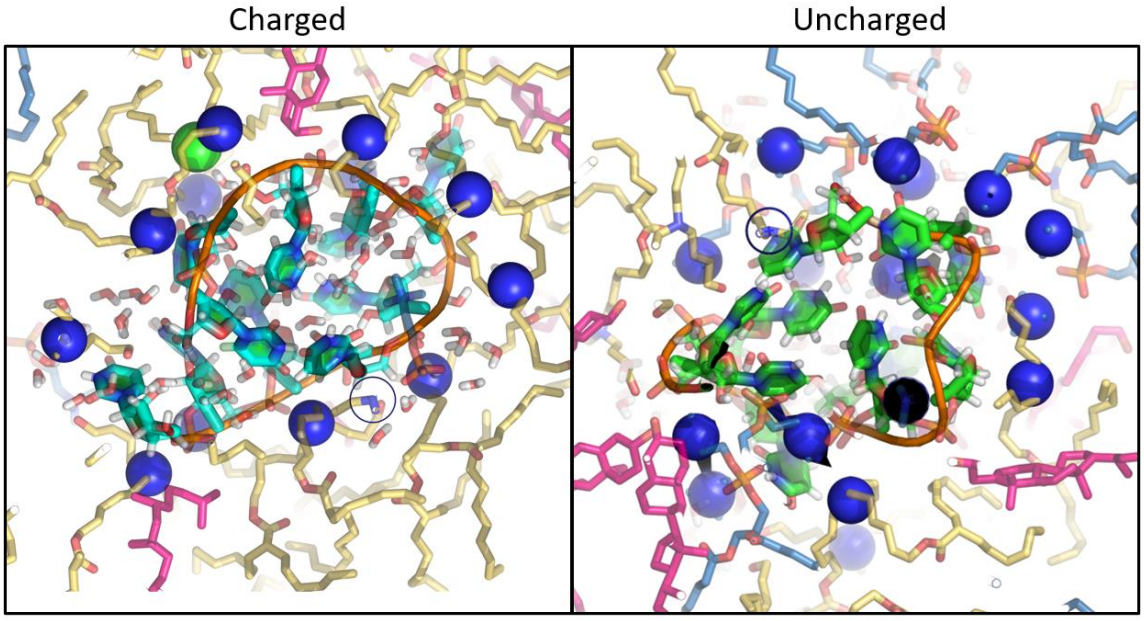

Figure S21*: Comparison of charged (left) and uncharged (right) simulations (oRNA-PEG-4000) focusing on single RNA backbone (yellow, cartoon) interacting with ILs (yellow), DSPC (blue) or cholesterol (magenta). Lipids and water are shown in sticks, lipid nitrogens are depicted as blue balls (circles in cross section).*

The RNA expulsion after the IL deprotonation can also be described as the change in the amount of RNA content within the LNP, as seen in Figures S22-S23. In the charged LNPs, all (100 %) RNA molecules were encapsulated in LNP. After the deprotonation, most of the RNA molecules leave the inner part of the particle and is released into the bulk water. After reprotonation, the RNA molecules return to the lipid environment, but the analysis is biased by structure connected via the periodic boundary conditions.

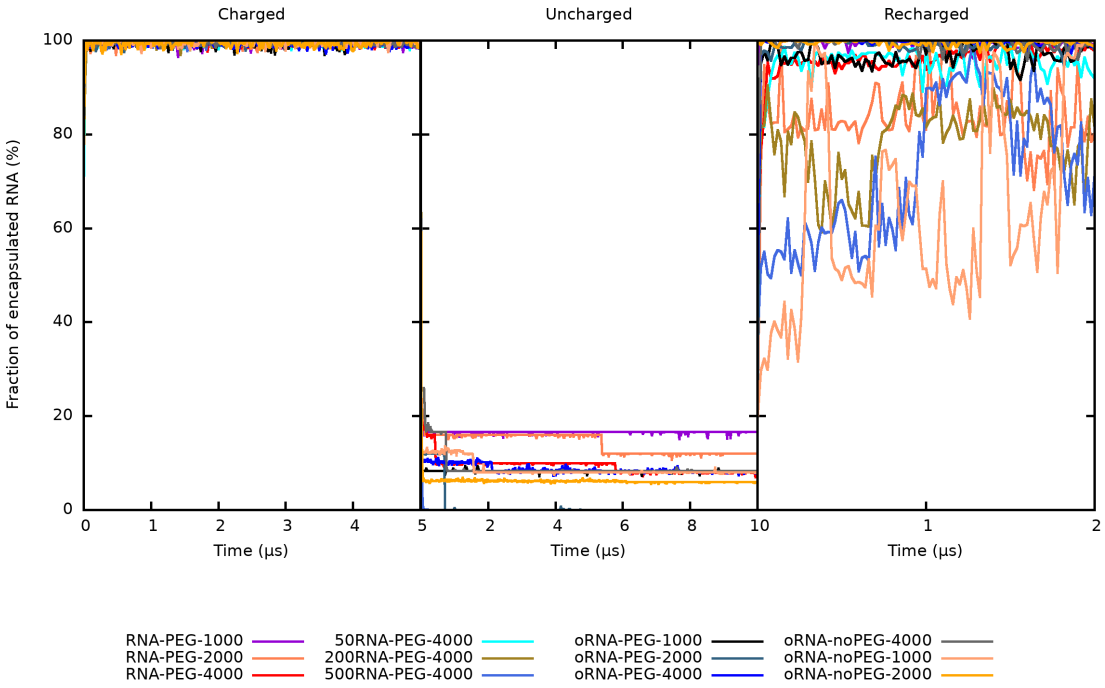

***Figure S22**: Fraction of RNA encapsulated inside the LNP calculated for each simulation (recharged systems are affected by formation of periodic aggregates instead of LNP).*

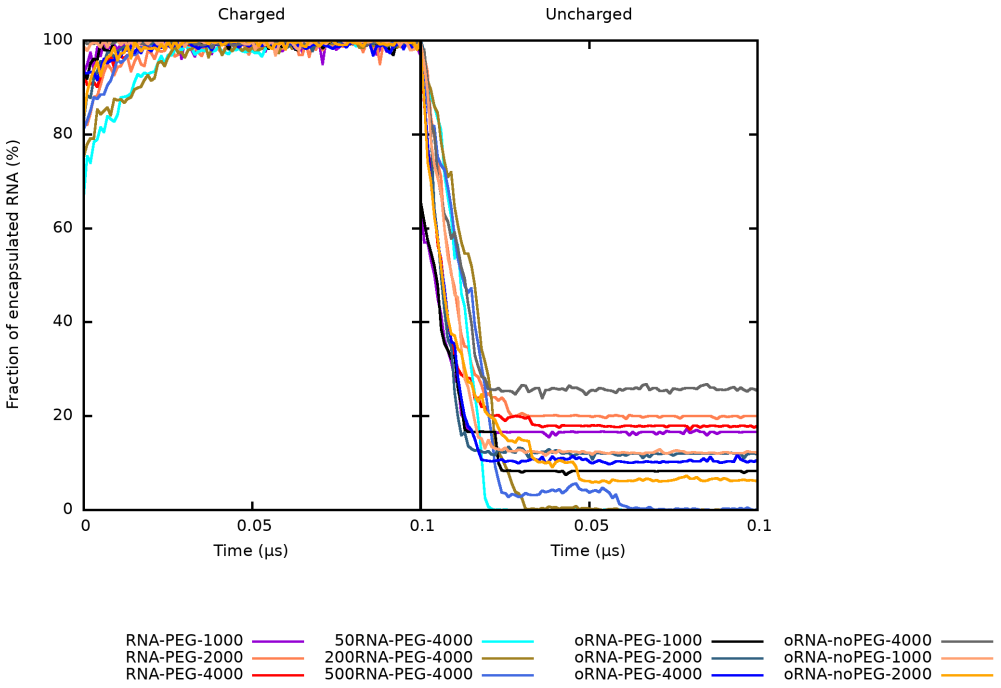

***Figure S23**: Fraction of RNA encapsulated in LNP during the first 100 ns of charged and uncharged simulations (detail analysis of the first 100 ns of Fig. S22). The majority of RNA is released during the first 20 ns after IL deprotonation (right)*

Final snapshots of all performed CG simulations

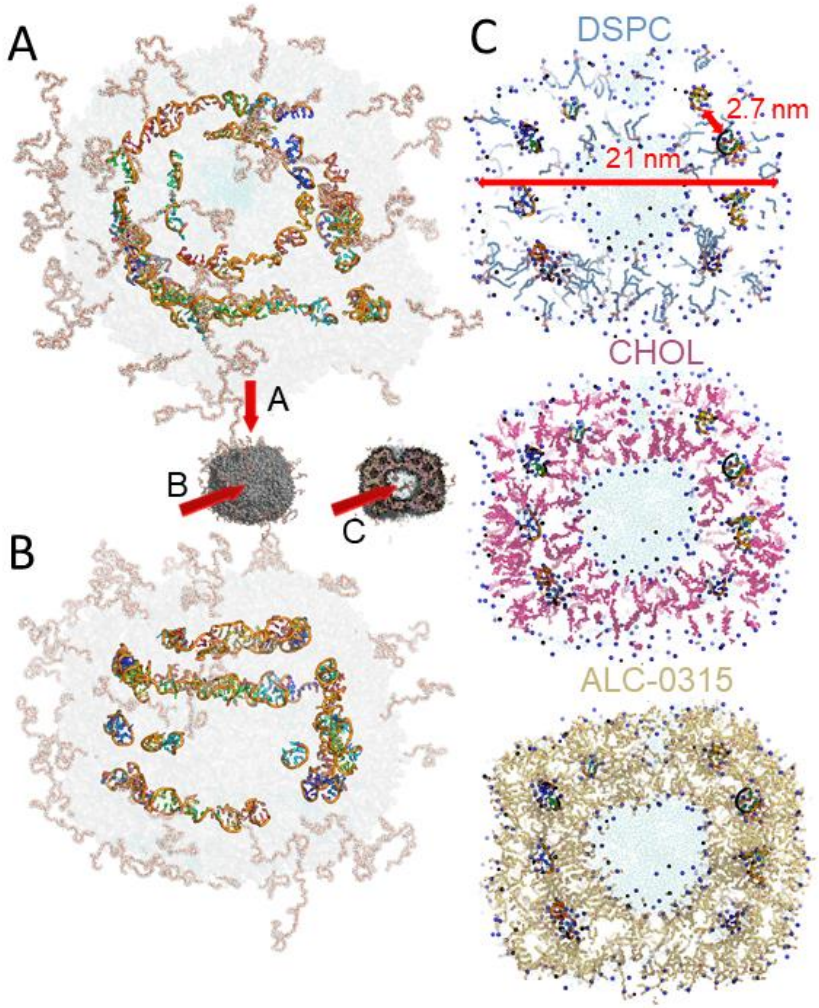

***Figure S24**: Top view (A) and side view (B) to the final snapshot of oRNA-PEG-4000 system with cross sections (C) highlighting individual lipids in hexagonal phase. ILs are displayed in yellow, cholesterol in magenta, DSPC in blue sticks and RNA as colored cartoon.*

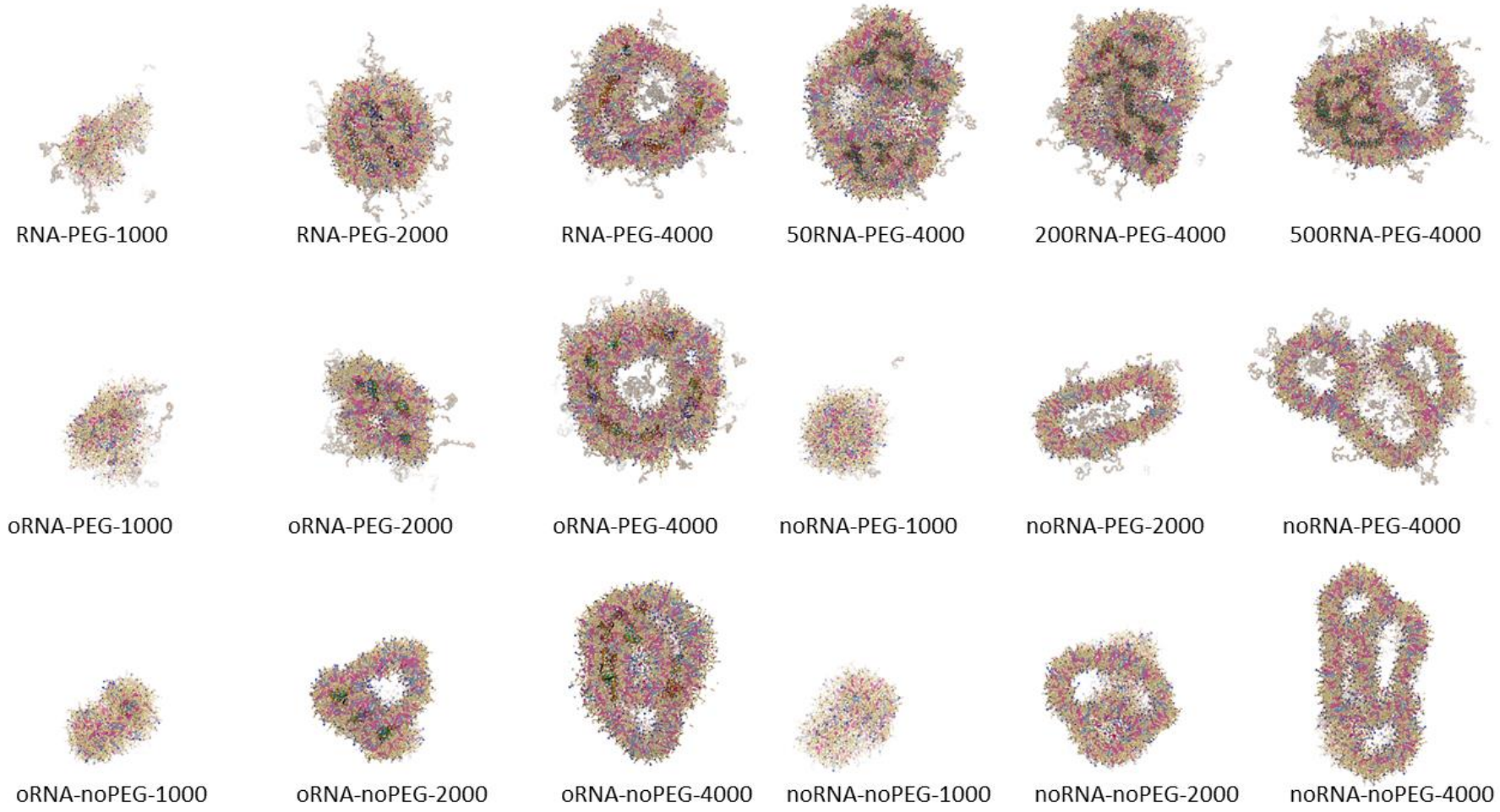

Figure S25*: Final conformation (cross section) of all systems in charged state after AA equilibration (10 ns). ILs are displayed in yellow, cholesterol in magenta, DSPC in blue sticks and RNA as green cartoon. Water and ions are omitted for clarity. The corresponding pdbs in CG and AA resolution are available in the data repository.*

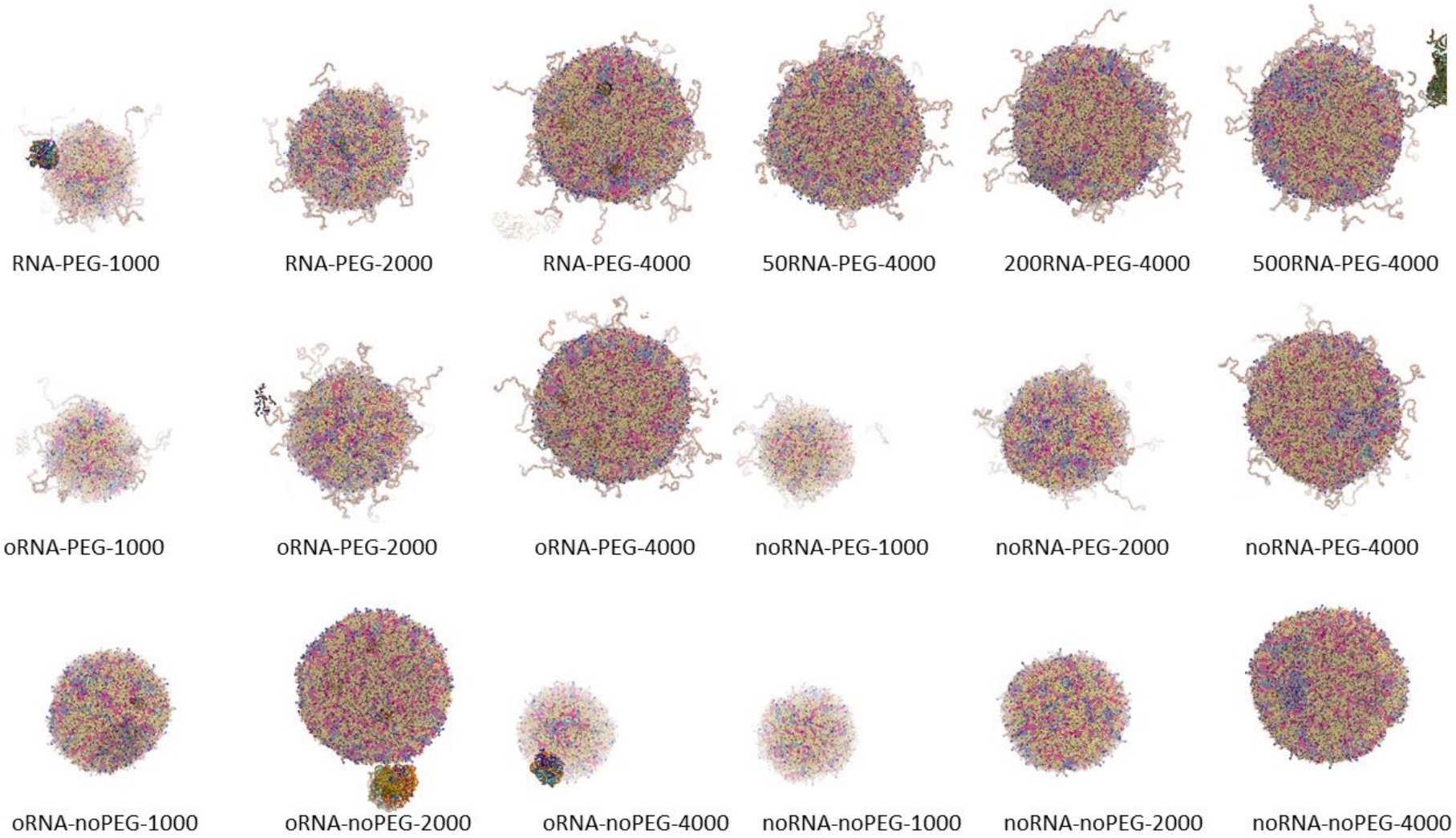

***Figure S26**: Final conformation (cross section) of all systems in uncharged state remapped into AA resolution. ILs are displayed in yellow, cholesterol in magenta, DSPC in blue sticks and RNA as green cartoon. Water and ions are omitted for clarity. The corresponding pdbs in CG and AA resolution are available in data repository.*

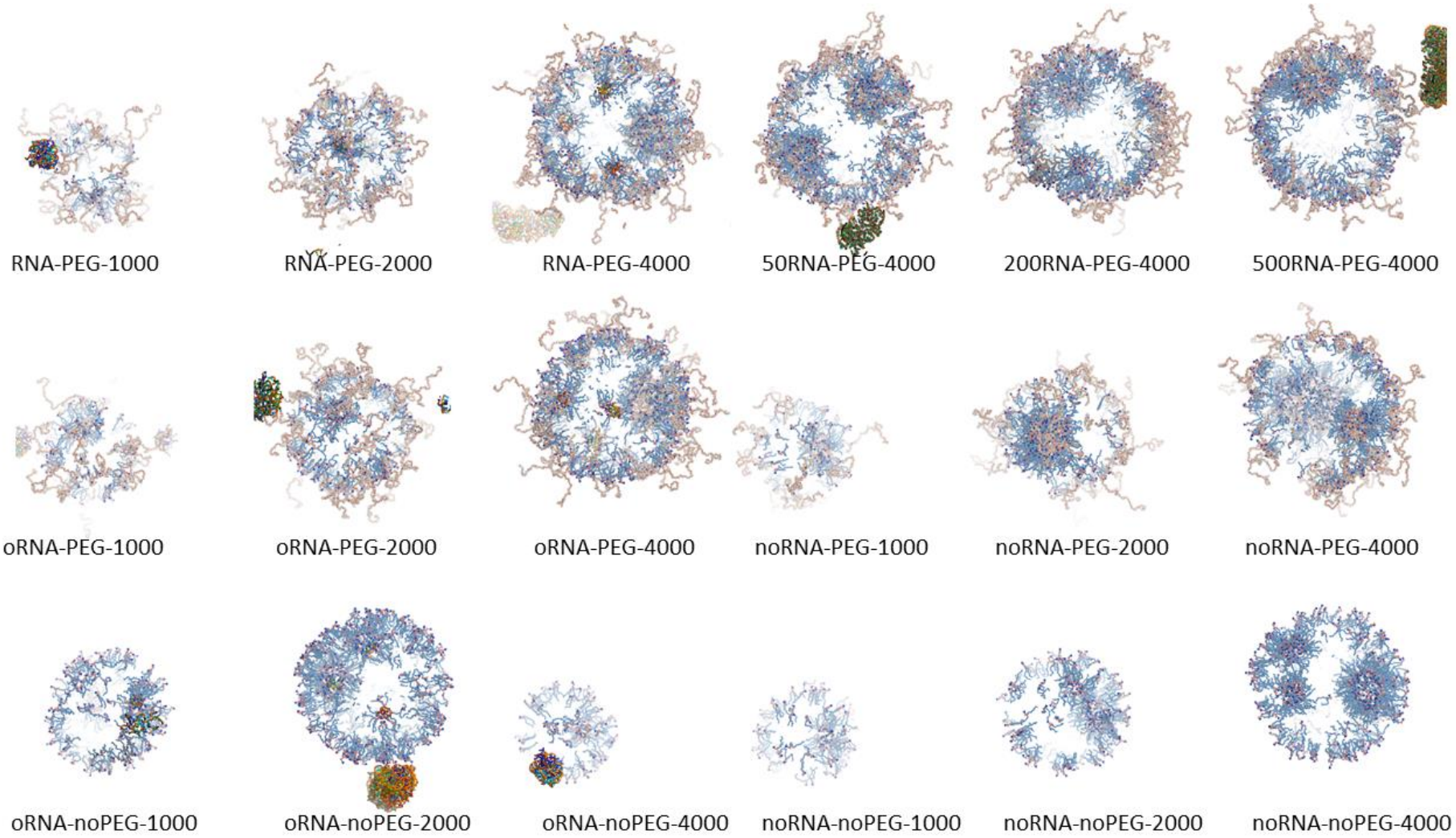

***Figure S27**: Final conformation (cross section) of all systems in uncharged state remapped into AA resolution. ILs and cholesterol are omitted, DSPC is displayed in blue sticks and RNA as green cartoon. Water and ions are omitted for clarity. The corresponding pdbs in CG and AA resolution are available in data repository.*

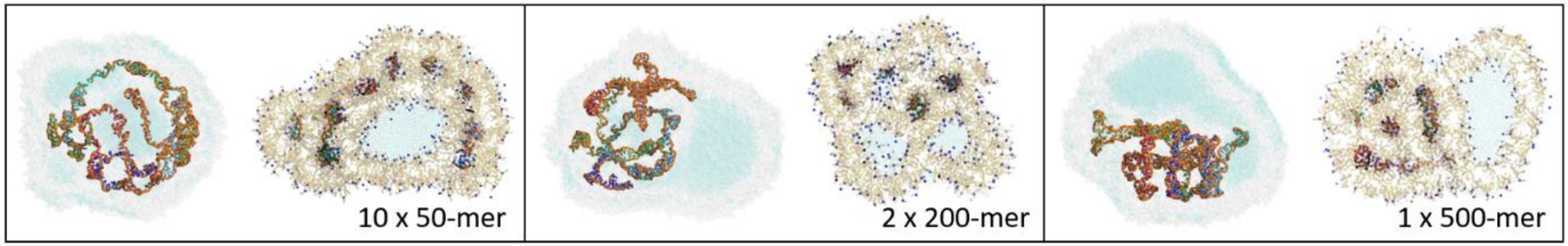

***Figure S28**: Structures of LNPs with long RNA chains (cartoon) with all lipids displayed as a transparent grey surface and internal waters as cyan dots (left). The right structures show a slice through the LNPs, highlighting the pattern of the hexagonal phase. ILs are displayed as yellow sticks and lipid nitrogens as blue balls.*

AA simulations

Protonated LNPs - polyU

To verify the results from CG simulations, we performed a 1 μs of MD simulation in all-atom resolution with the same simulations setup as in CG resolution – randomly inserting lipids and RNA into a simulation box and hydrating them, followed by simulated annealing simulation. Due to the used AA resolution, we used a smaller system (400 lipids) and monitored the formation of LNP. RNA gradually incorporated into LNP and remained in contact with lipids and internal water droplet (*Figure S29*). The first solvation shell in the radial distribution function (RDF, *Figure S30*) was very similar to that of large-scale structures (*Figure 1*) as well as the distribution of hydrogen bonds between lipids and RNA (Figures S33-36). However, due to the size of the AA LNP, we could not observe another RNA in hexagonal phase and the second peak of lipid head groups (~4 nm) was already due to LNP surface. Overall, our AA simulations confirmed the reliability of CG results on large scale.

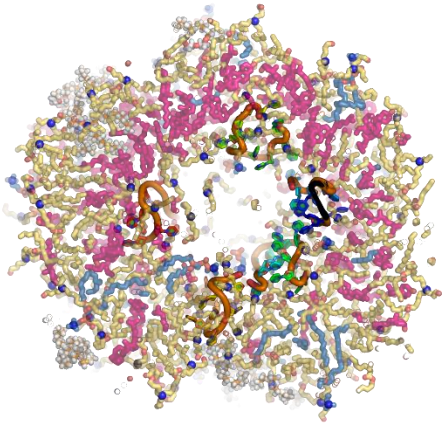

***Figure S29**: Final structure of LNP assembled in AA resolution (cross section). RNA is displayed as cartoon, ILs in yellow stick, DSPC in blue, cholesterol in magenta and PEGylated lipids in orange. IL and DSPC nitrogens are shown in blue balls. Water and ions are omitted for clarity.*

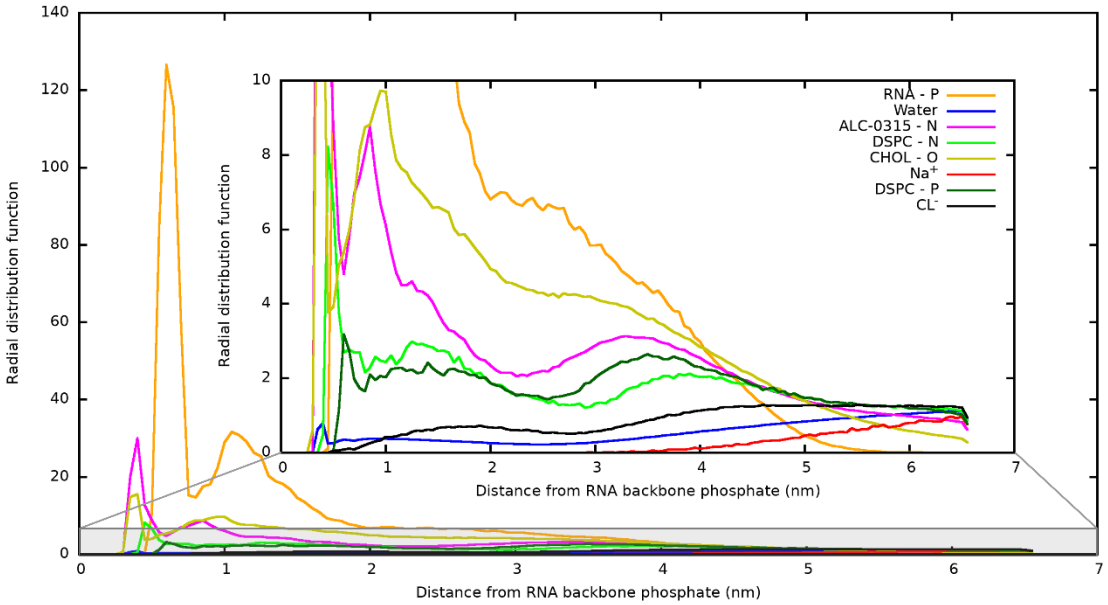

***Figure S30**: Radial distribution function of individual atoms around RNA backbone phosphates calculated in AA simulation. The analysis was performed on the last 500 ns of the atomistic simulation. The grey rectangle shows the region covered by the inset.*

Protonated LNP with dengue virus stem-loop RNA

The self-assembly snapshots (Figure S31) and RDF values of each stem-loop RNA (Figure S32) molecules corroborate the behavior of the coarse-grained and AA polyU systems.

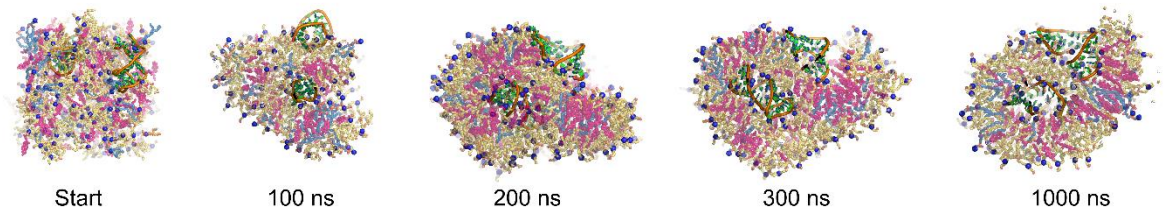

***Figure S31**: Cross section of snapshots of AA simulation of LNP formation with dengue virus stem-loop RNA. No significant changes in the structure were observed after 1 μs. RNA is displayed as cartoon, ILs in yellow stick, DSPC in blue, cholesterol in magenta. IL and DSPC nitrogens are shown in blue balls. Water, ions, and PEGylated lipids are omitted for clarity.*

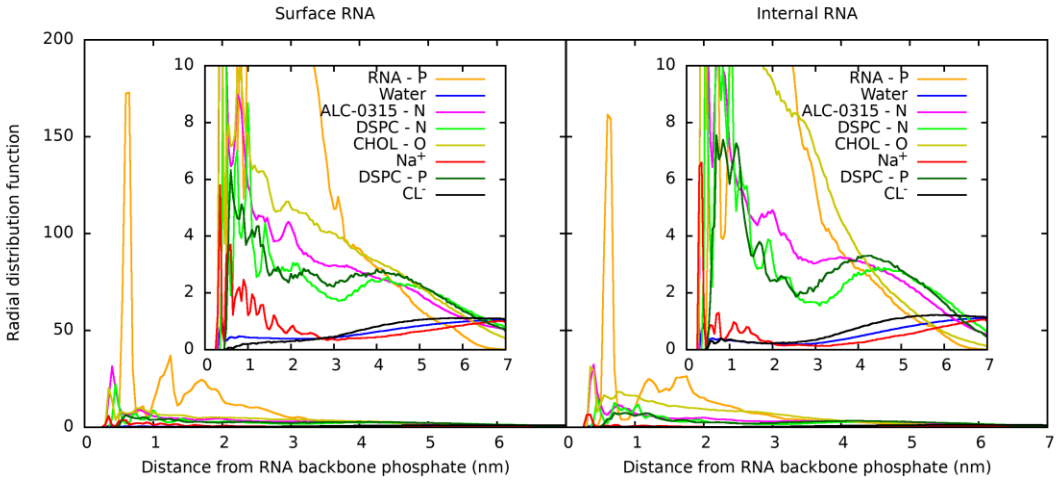

***Figure S32**: Radial distribution function of individual atoms around RNA backbone phosphates calculated in AA simulation, separately for surface and internal stem-loop RNAs. The analysis was performed on the last 500 ns of the atomistic simulation. The insets show a zoomed area of the background plot.*

Hydrogen bonds analysis

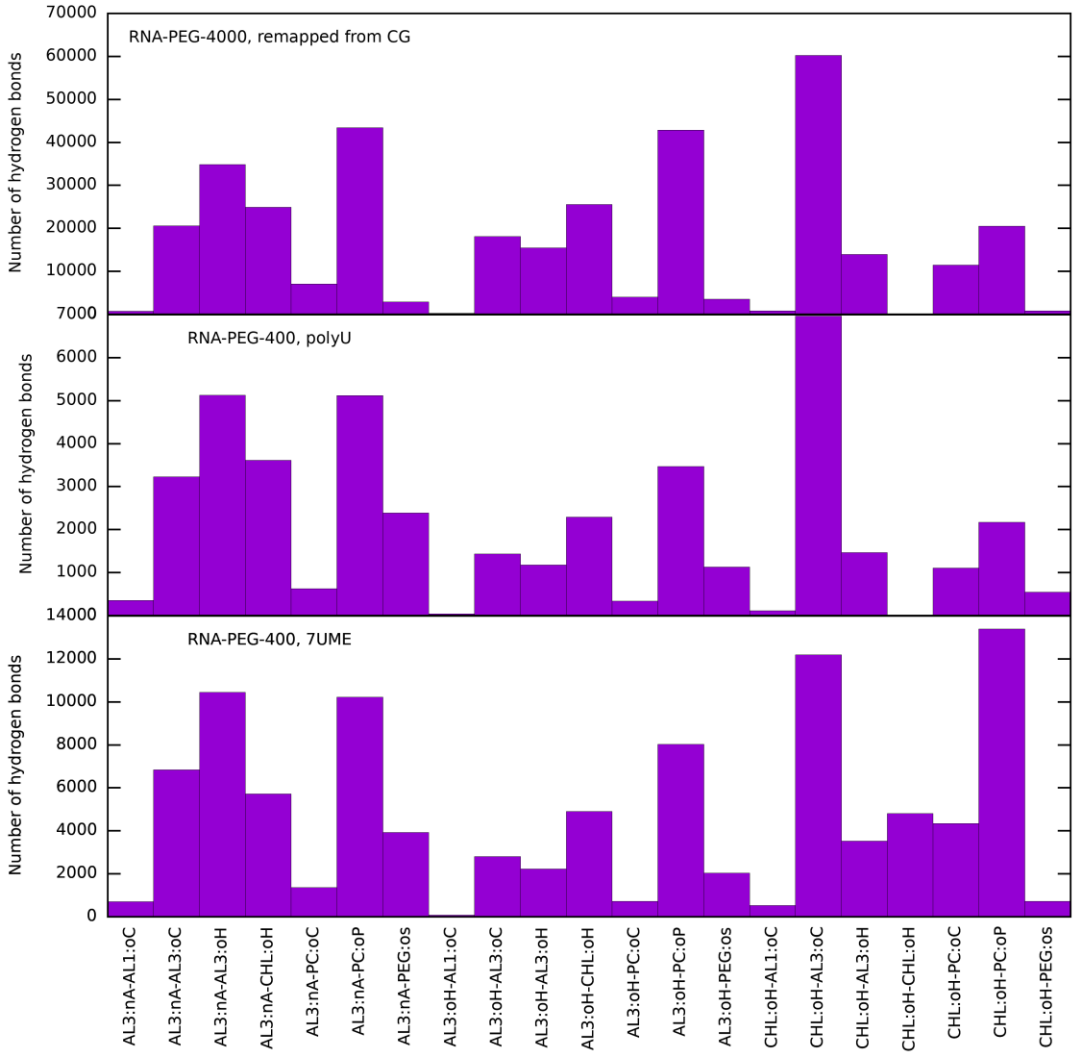

Figure S33*: Number of hydrogen bonds between lipid components in the 10 ns simulation after remapping of CG structure of RNA-PEG-4000 (upper panel) and in 1 μs of a self-assembly LNP with polyU chain (middle) and in 2 μs simulation of two 7UME hairpins (lower panel). The ratio between individual components remains preserved in all systems with the exception of increased fraction of hydrogen bonds between CHOL and DSPC surrounding 7UME chains, suggesting possible clustering. Group naming:ALC-0315 (IL): AL3:nA – amino group, AL3:oH – hydroxyl group, AL3:oC – ester group; ALC-0159 (PEGylated lipid): AL1:oC – carbonyl group, PEG:oS – PEG oxygen; Cholesterol: CHL:oH – hydroxyl group; PC: oC – carbonyl group, PC:oP – phosphate oxygens*

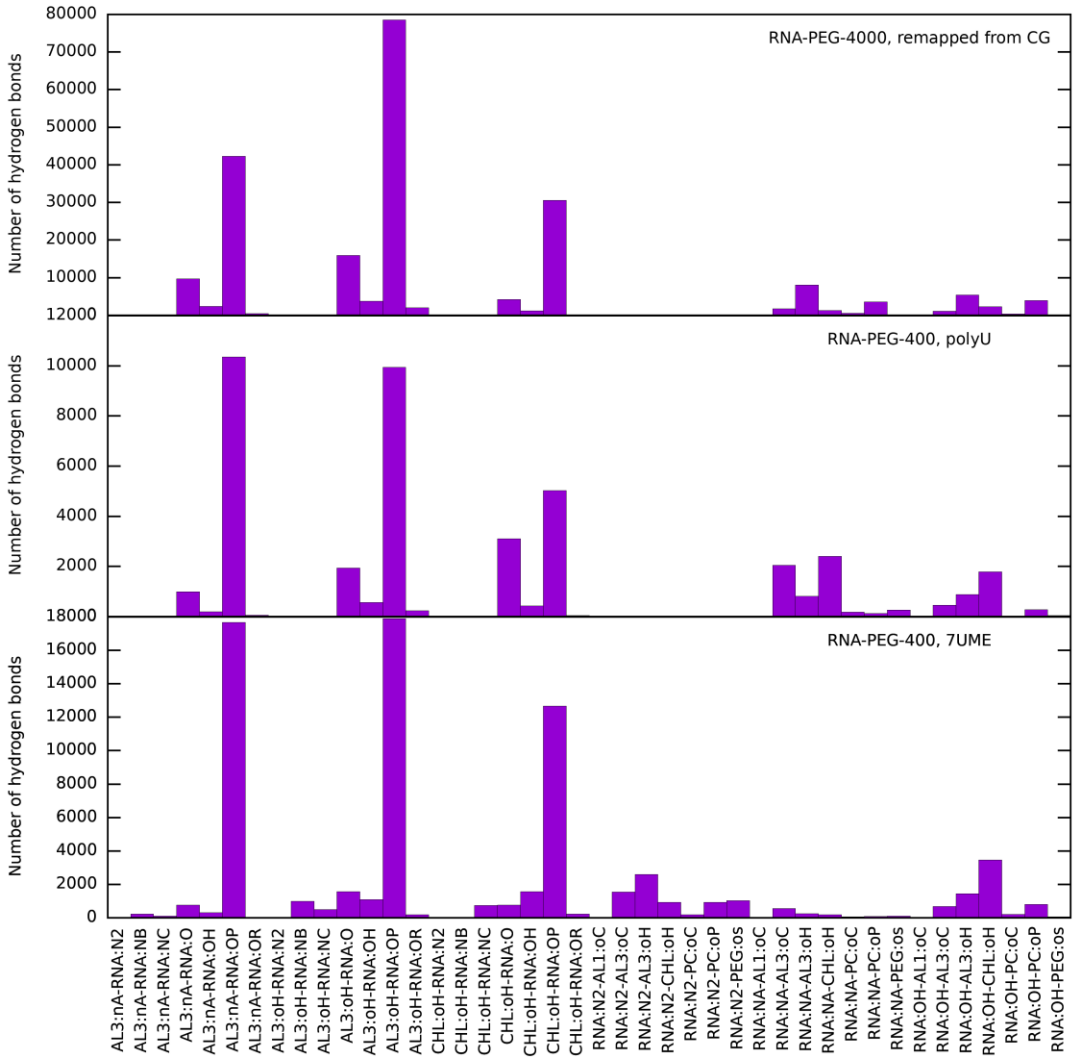

Figure S34*: Number of hydrogen bonds between RNA and lipid components in the 10 ns simulation after remapping of CG structure of RNA-PEG-4000 (upper panel) and in 1 μs of a self-assembly LNP with polyU chain (middle) and in 2 μs simulation of two 7UME hairpins (lower panel). The ratio between individual components and the most abundant hydrogen bonds remains preserved in all systems. The most abundant hydrogen bonds are between IL amino and hydroxyl group and RNA phosphate oxygens, and between cholesterol hydroxyl group and RNA phosphate oxygen. In polyU RNA:N2 group is not present and therefore the ratio of lipid-RNA hydrogen bonds of RNA bases is different in 7UME and polyU chains. Group naming:ALC-0315 (IL): AL3:nA – amino group, AL3:oH – hydroxyl group, AL3:oC – ester group; ALC-0159 (PEGylated lipid): AL1:oC – carbonyl group, PEG:oS – PEG oxygen; Cholesterol: CHL:oH – hydroxyl group; PC: oC – carbonyl group, PC:oP – phosphate oxygens; Nucleic acid: RNA:NA – pyrrole-like NH group, RNA:N2 – amino groups, RNA:OH – ribose hydroxyl, RNA: NB, NC – aromatic pyridine-like nitrogens, RNA:O – carbonyls on bases, RNA:OP – phosphate oxygens, RNA:OR – 03' and 05' oxygens*

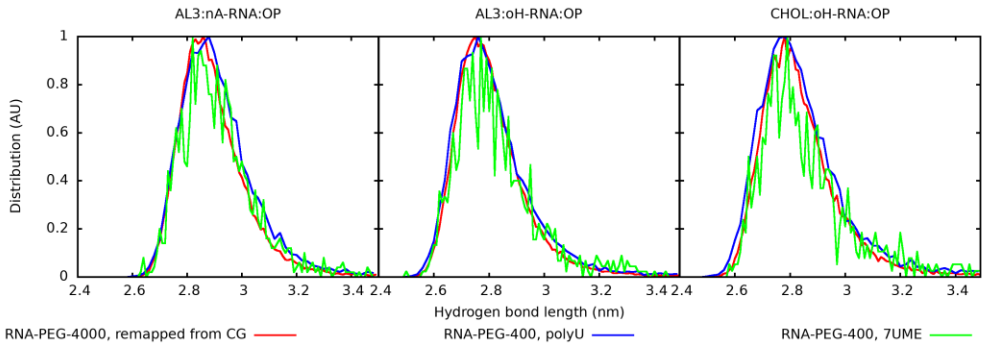

***Figure S35**: Distribution of the lengths of the most abundant hydrogen bonds from Figure S34. The hydrogen bonds in systems from AA and CG simulations are identical.*

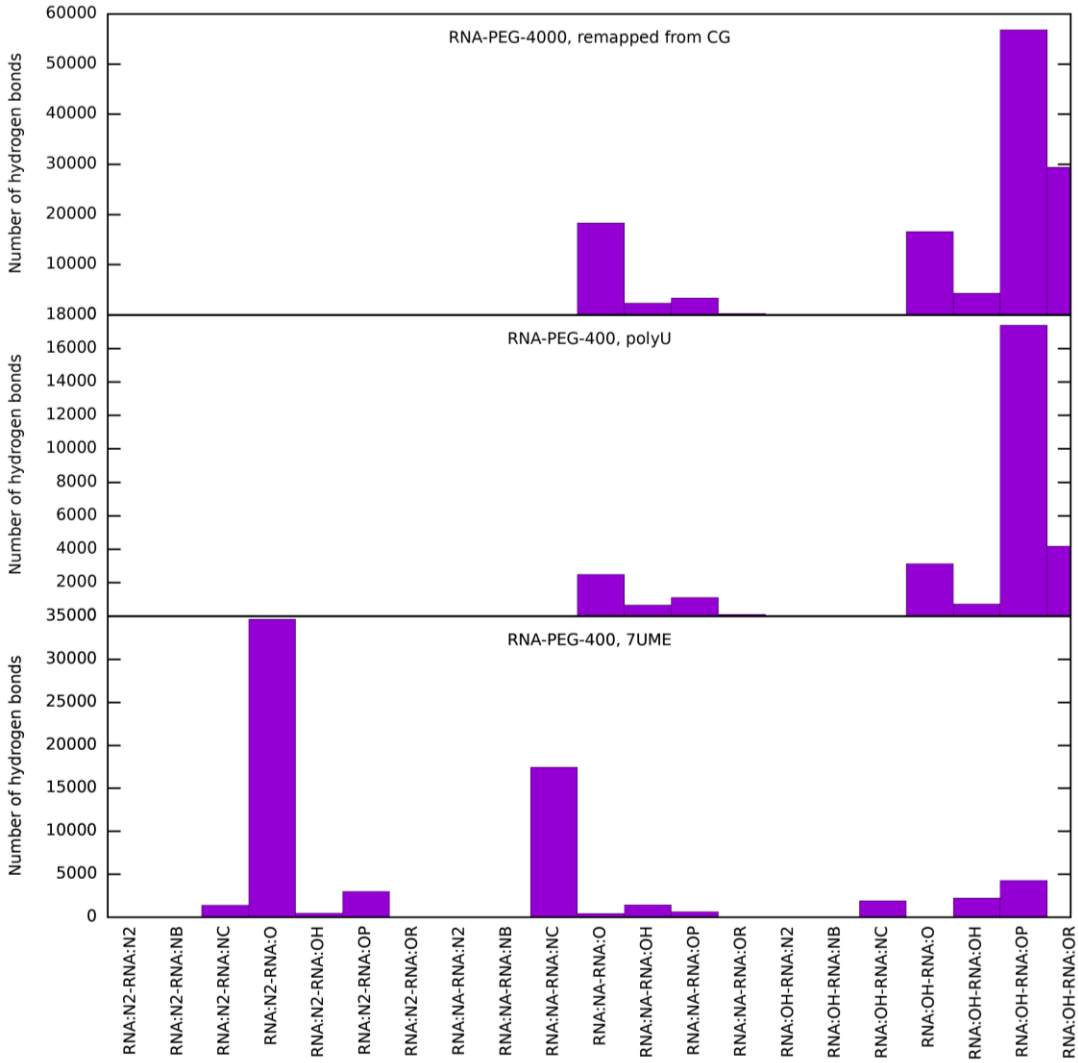

***Figure S36**: Number of hydrogen bonds between RNA groups in the 10 ns simulation after remapping of CG structure of RNA-PEG-4000 (upper panel) and in 1 μs of a self-assembly LNP with polyU chain (middle) and in 2 μs simulation of two 7UME hairpins (lower panel). The structure of 7UME hairpin and unstructured polyU chain is very different, therefore the hydrogen bonds distribution differs. Group naming: Nucleic acid: RNA:NA – pyrrole-like NH group, RNA:N2 – amino groups, RNA:OH – ribose hydroxyl, RNA: NB, NC – aromatic pyridine-like nitrogens, RNA:O – carbonyls on bases, RNA:OP – phosphate oxygens, RNA:OR – 03' and 05' oxygens*

Deprotonated LNP in AA resolution

In order to validate the observed response of LNP to IL deprotonation, we simulated this process in AA resolution. We remapped the final LNP structure from RNA-PEG-1000 in charged state into deprotonated AA structure and performed 500 ns of MD simulation (with simulated annealing). In agreement with the CG simulations, we observed reshaping of LNP into a more spherical particle, its dehydration and a spontaneous repelling of RNA molecules from LNP, as the negatively charged RNA lost its favorable interactions with positively charged ILs. During 500 ns of simulation, the RNA molecules were expelled to the LNP surface and started to preferentially interact with water instead of LNP (*Figure S37*). While in CG simulation, the reshaping of LNP happens within ns units and most of the RNA expelling during the first 20 ns of simulation, in AA simulation all these processes are slower. The reshaping of LNP took ~ 50 ns, while the expelling of RNA was still in process after 500 ns of simulation with ~20 % of RNA still remaining inside LNP. Due to the rather short simulation time and slower diffusion in AA resolution, we did not observe full phase separation between lipid types, but the phase separation of lipids has been already described in longer simulations of lipid bilayers.[3]

Concludingly, all simulations performed in AA resolution fully support the observations in CG resolution and the CG models can therefore be taken as reliable models and extended for very large scale simulations, unavailable in AA resolution.

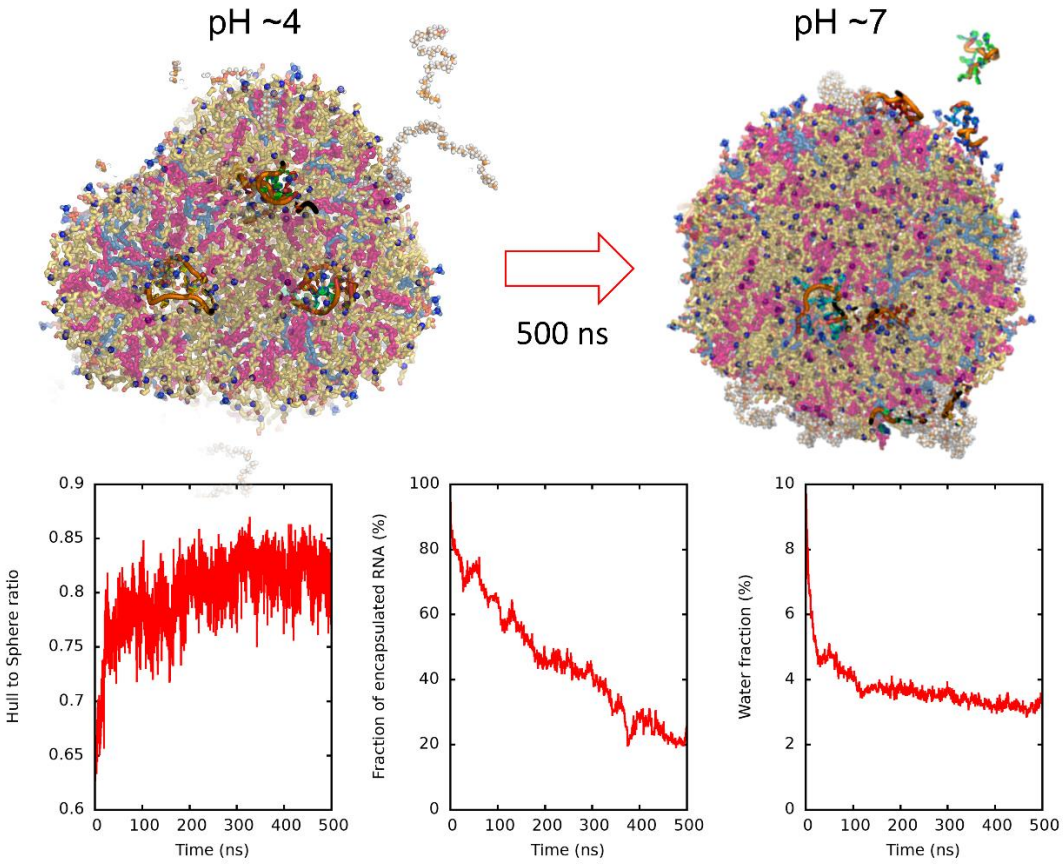

***Figure S37**: Initial (left) and final (right) structure of RNA-PEG-1000 remapped into AA resolution with uncharged ILs. Lower panel: During the simulations, LNP adjusted its shape to more spherical particle, as seen at a ratio of LNP convex hull surface area to a surface area of a perfect sphere (left). RNA was gradually expelled from LNP (middle) as well as water content (right). RNA is displayed as cartoon, ILs in yellow stick, DSPC in blue, cholesterol in magenta and PEGylated lipids in orange. IL and DSPC nitrogens are shown in blue balls. Water and ions are omitted for clarity.*

RNA characteristics

In all simulations, regardless of the size of the system, the RNA showed the same type of behavior. RNA conformation was dominated by base-stacking interactions, with more than half of the bases interacting with other bases via base-stacking. The bases themselves paired very little with each other, i.e. base-pairing was only represented to a small extent. The lipids presence had a major effect on the dihedral conformational space of the RNA backbone, with the backbone having only a very limited ability to adopt any of the defined conformations and the vast majority of dihedral angels not belonging to any of the conformational families described.

***Table S8**: Number of base-pairs, base-stacks, and percentage of well-classified backbone conformation calculated per frame for all simulations containing RNA.*

System	Number of bases	Base-pairing	Base-stacking	Backbone conformation
		#pairs	#stacks	%
RNA-PEG-1000	120	3	68	2
RNA-PEG-2000	250	2	141	2
RNA-PEG-4000	500	8	295	2
50RNA-PEG-4000	500	10	296	2
200RNA-PEG-4000	400	5	236	3
500RNA-PEG-4000	500	11	305	2
oRNA-PEG-1000	120	3	76	3
oRNA-PEG-2000	250	6	170	2
oRNA-PEG-4000	500	12	307	3
oRNA-noPEG-1000	120	4	70	2
oRNA-noPEG-2000	250	3	143	2
oRNA-noPEG-4000	500	11	306	3

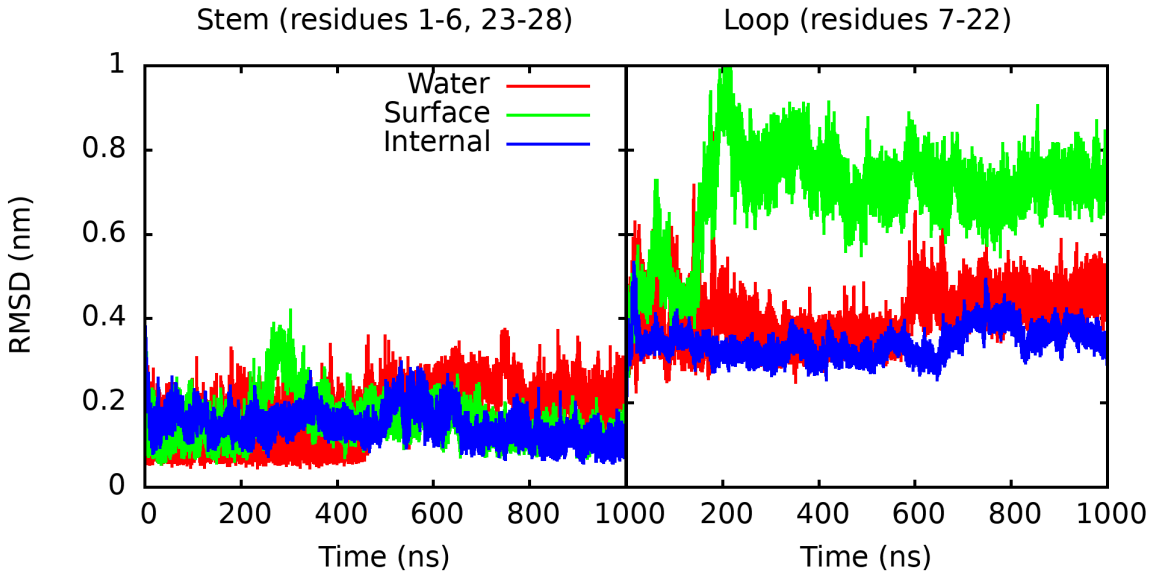

***Figure S38**: Root mean square deviations of backbone atoms of viral RNA stem (left) and loop (right) in the simulations of RNA in water (red) and in LNP for surface (green) and internal (blue) RNA in respect to the starting structure (NMR structure). The stem of surface RNA is embedded in lipid matrix and is stabilized by lipids in the similar manner as in the case of internal RNA, while the loop of surface RNA is distorted by the water/lipids interface.*

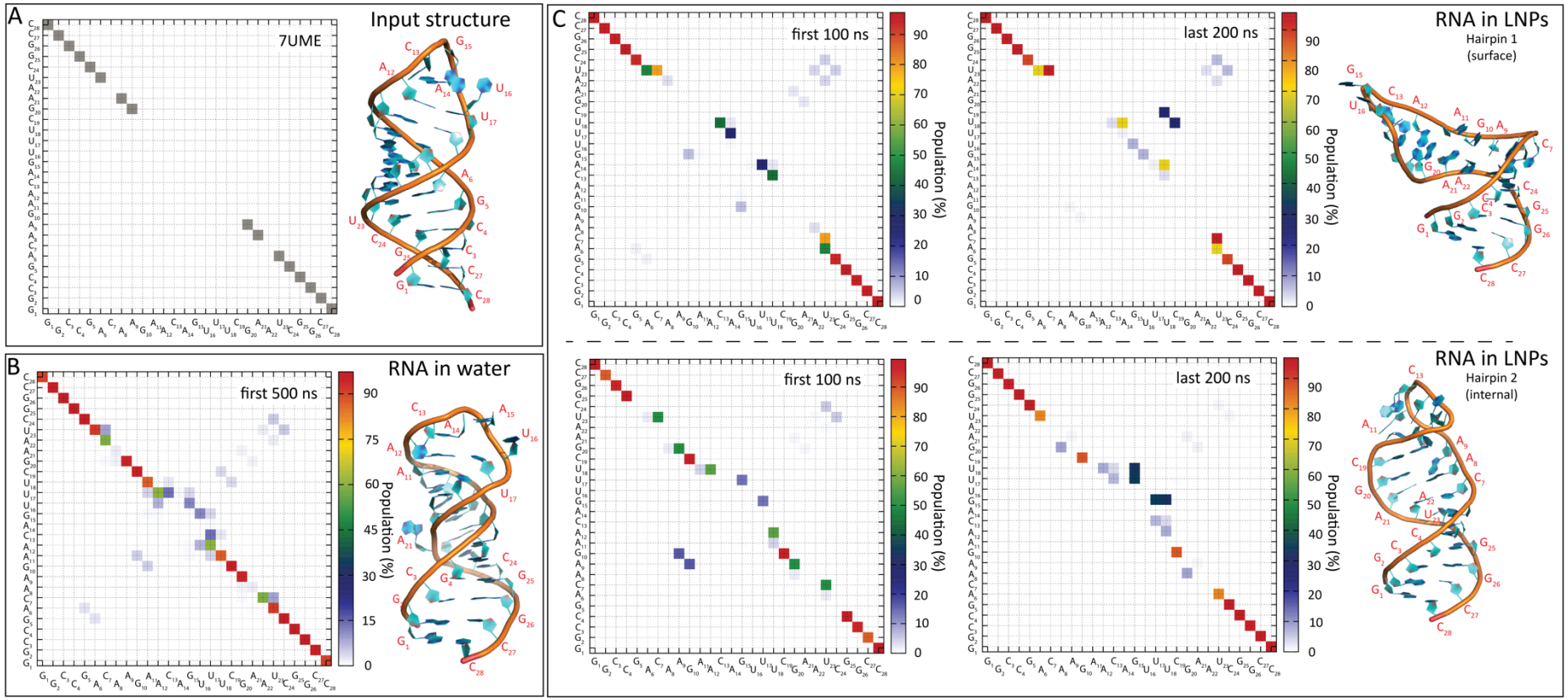

***Figure S39**: Interaction matrixes showing base pairing of hairpin from the dengue virus in A) NMR structure 7UME[15] (frame 1); B) simulated annealing-MD simulations performed only in water; C) MD simulation in the presence of LNPs. This simulation contained two hairpins. Hairpin 1 was present on the surface of the nanoparticle during the simulation while Hairpin 2 was inside the nanoparticle at all simulation times. All states were clustered according to family of edge-to-edge base-pairs between all bases and were classified according to ref. [16]. The color scale represents the population of snapshots during simulations in which base pair interact, ranging from zero (white) to high (red) propensity of base pairing.*

Bibliography

(1) Souza, P. C. T.; Alessandri, R.; Barnoud, J.; Faustino, I.; Grunewald, F.; Patmanidis, I.; Thallmair, S.; Faustino, I.; Grünewald, F.; Patmanidis, I.; Abdizadeh, H.; Bruininks, B. M. H.; Wassenaar, T. A.; Kroon, P. C.; Melcr, J.; Nieto, V.; Corradi, V.; Khan, H. M.; Domański, J.; Javanainen, M.; Martinez-Seara, H.; Reuter, N.; Best, R. B.; Vattulainen, I.; Monticelli, L.; Periole, X.; Tieleman, D. P.; de Vries, A. H.; Marrink, S. J. Martini 3 : A General Purpose Force Field for Coarse-Grained Molecular Dynamics. *Nat. Methods* **2021**, *18* (4), 382–388. https://doi.org/10.1038/s41592-021-01098-3.

(2) Schoenmaker, L.; Witzigmann, D.; Kulkarni, J. A.; Verbeke, R.; Kersten, G.; Jiskoot, W.; Crommelin, D. J. A. MRNA-Lipid Nanoparticle COVID-19 Vaccines: Structure and Stability. *Int. J. Pharm.* **2021**, *601* (April), 120586. https://doi.org/10.1016/j.ijpharm.2021.120586.

(3) Paloncýová, M.; Čechová, P.; Šrejber, M.; Kührová, P.; Otyepka, M. Role of Ionizable Lipids in SARS-CoV-2 Vaccines As Revealed by Molecular Dynamics Simulations: From Membrane Structure to Interaction with MRNA Fragments. *J. Phys. Chem. Lett.* **2021**, *12* (45), 11199–11205. https://doi.org/10.1021/acs.jpclett.1c03109.

(4) Grünewald, F.; Alessandri, R.; Kroon, P. C.; Monticelli, L.; Souza, P. C. T.; Marrink, S. J. Polyply; a Python Suite for Facilitating Simulations of Macromolecules and Nanomaterials. *Nat. Commun.* **2022**, *13* (1), 1–19. https://doi.org/10.1038/s41467-021-27627-4.

(5) Tsanai, M.; Frederix, P. W. J. M.; Schroer, C. F. E.; Souza, P. C. T.; Marrink, S. J. Coacervate Formation Studied by Explicit Solvent Coarse-Grain Molecular Dynamics with the Martini Model. *Chem. Sci.* **2021**, *12* (24), 8521–8530. https://doi.org/10.1039/d1sc00374g.

(6) Hornak, V.; Abel, R.; Okur, A.; Strockbine, B.; Roitberg, A.; Simmerling, C. Comparison of Multiple Amber Force Fields and Development of Improved Protein Backbone Parameters. *Proteins Struct. Funct. Bioinforma.* **2006**, *65* (May), 712–725. https://doi.org/10.1002/prot.

(7) Zgarbová, M.; Otyepka, M.; Šponer, J.; Mládek, A.; Banáš, P.; Cheatham, T. E.; Jurečka, P. Refinement of the Cornell et Al. Nucleic Acids Force Field Based on Reference Quantum Chemical Calculations of Glycosidic Torsion Profiles. *J. Chem. Theory Comput.* **2011**, *7* (9), 2886–2902. https://doi.org/10.1021/ct200162x.

(8) Pérez, A.; Marchán, I.; Svozil, D.; Sponer, J.; Cheatham, T. E.; Laughton, C. A.; Orozco, M. Refinement of the AMBER Force Field for Nucleic Acids: Improving the Description of α/γ Conformers. *Biophys. J.* **2007**, *92* (11), 3817–3829. https://doi.org/10.1529/biophysj.106.097782.

(9) Steinbrecher, T.; Latzer, J.; Case, D. A. Revised AMBER Parameters for Bioorganic Phosphates. *J. Chem. Theory Comput.* **2012**, *8* (11), 4405–4412. https://doi.org/10.1021/ct300613v.

(10) Michaud-Agrawal, N.; Denning, E. J.; Woolf, T. B.; Beckstein, O. MDAnalysis: A Toolkit for the Analysis of Molecular Dynamics Simulations. *J. Comput. Chem.* **2011**, *32* (10), 2319–2327. https://doi.org/10.1002/jcc.21787.

(11) Smith, P.; Lorenz, C. D. LiPyphilic: A Python Toolkit for the Analysis of Lipid Membrane Simulations. *J. Chem. Theory Comput.* **2021**, *17* (9), 5907–5919. https://doi.org/10.1021/acs.jctc.1c00447.

(12) Rycroft, C. H. VORO++: A Three-Dimensional Voronoi Cell Library in C++. *Chaos An Interdiscip. J. Nonlinear Sci.* **2009**, *19* (4), 041111. https://doi.org/10.1063/1.3215722.

(13) Abel, S.; Dupradeau, F.-Y.; Marchi, M. Molecular Dynamics Simulations of a Characteristic DPC Micelle in Water. *J. Chem. Theory Comput.* **2012**, *8* (11), 4610–4623. https://doi.org/10.1021/ct3003207.

(14) Ingólfsson, H. I.; Melo, M. N.; Van Eerden, F. J.; Arnarez, C.; Lopez, C. A.; Wassenaar, T. A.; Periole, X.; De Vries, A. H.; Tieleman, D. P.; Marrink, S. J. Lipid Organization of the Plasma Membrane. *J. Am. Chem. Soc.* **2014**, *136* (41), 14554–14559. https://doi.org/10.1021/ja507832e.

(15) Sun, Y.-T.; Varani, G. Structure of the Dengue Virus RNA Promoter. *RNA* **2022**, *28* (9), 1210–1223. https://doi.org/10.1261/rna.079197.122.

(16) LEONTIS, N. B.; WESTHOF, E. Geometric Nomenclature and Classification of RNA Base Pairs. *RNA* **2001**, *7* (4), S1355838201002515. https://doi.org/10.1017/S1355838201002515.